NASA TECHNICAL NOTE

NASA TN D-8323

CORRELATION OF FULL-SCALE HELICOPTER ROTOR PERFORMANCE IN AIR WITH MODEL-SCALE FREON DATA

William T. Yeager, Jr., and Wayne R. Mantay

Langley Research Center
Hampton, Va. 23665

NATIONAL AERONAUTICS AND SPACE ADMINISTRATION • WASHINGTON, D. C. • NOVEMBER 1976

1. Report No.	2. Government Accession No.	3. Recipient's Catalog No.
NASA TN D-8323		

4. Title and Subtitle	5. Report Date
CORRELATION OF FULL-SCALE HELICOPTER ROTOR PERFORMANCE IN AIR WITH MODEL-SCALE FREON DATA	November 1976
	6. Performing Organization Code
7. Author(s)	8. Performing Organization Report No.
William T. Yeager, Jr., and Wayne R. Mantay	L-10844
	10. Work Unit No. 505-10-21-03
9. Performing Organization Name and Address NASA Langley Research Center and Langley Directorate, USAAMRDL Hampton, VA 23665	11. Contract or Grant No.
	13. Type of Report and Period Covered Technical Note
12. Sponsoring Agency Name and Address National Aeronautics and Space Administration Washington, DC 20546 and U.S. Army Air Mobility R&D Laboratory Moffett Field, CA 94035	14. Army Project No. 1F161102AH45

15. Supplementary Notes

William T. Yeager, Jr., and Wayne R. Mantay: Langley Directorate, U.S. Army Air Mobility R&D Laboratory.

16. Abstract

An investigation was conducted in the Langley transonic dynamics tunnel to measure the performance of a $\frac{1}{5}$-scale model helicopter rotor in a freon atmosphere. Comparisons were made between these data and full-scale data obtained in air. Both the model and full-scale tests were conducted at advance ratios between 0.30 and 0.40 and advancing tip Mach numbers between 0.79 and 0.95.

Results show that correlation of model-scale rotor performance data obtained in freon with full-scale rotor performance data in air is good with regard to data trends. Mach number effects were found to be essentially the same for the model rotor performance data obtained in freon and the full-scale rotor performance data obtained in air. It was determined that Reynolds number effects may be of the same magnitude or smaller than rotor solidity effects or blade elastic modeling in rotor aerodynamic performance testing.

These results should prove useful to the rotary-wing industry since they indicate that by testing in a freon atmosphere, smaller less expensive models may be used to obtain meaningful rotor performance data.

17. Key Words (Suggested by Author(s))	18. Distribution Statement
Freon Reynolds number Model rotor testing Dynamic scaling Solidity corrections Rotor performance correlation	Unclassified – Unlimited Subject Category 02

19. Security Classif. (of this report)	20. Security Classif. (of this page)	21. No. of Pages	22. Price*
Unclassified	Unclassified	59	$4.25

* For sale by the National Technical Information Service, Springfield, Virginia 22161

CORRELATION OF FULL-SCALE HELICOPTER ROTOR PERFORMANCE IN AIR WITH MODEL-SCALE FREON DATA

William T. Yeager, Jr.,* and Wayne R. Mantay*
Langley Research Center

SUMMARY

An investigation was conducted in the Langley transonic dynamics tunnel to measure the performance of a $\frac{1}{5}$-scale model helicopter rotor in a freon atmosphere. Comparisons were made between these data and full-scale data obtained in air. Both the model and full-scale tests were conducted at advance ratios between 0.30 and 0.40 and advancing tip Mach numbers between 0.79 and 0.95.

Results show that correlation of model-scale rotor performance data obtained in freon with full-scale rotor performance data in air is good with regard to data trends. Mach number effects were found to be essentially the same for the model rotor performance data obtained in freon and the full-scale rotor performance data obtained in air. It was determined that Reynolds number effects may be of the same magnitude or smaller than rotor solidity effects or blade elastic modeling in rotor aerodynamic performance testing.

INTRODUCTION

The development of new rotor systems for advanced helicopters will require extensive analysis and testing. At present, wind-tunnel testing of full-scale rotor systems at moderate to high advance ratios is subject to tunnel-speed limitations, while testing at model scale in air does not lend itself to a simultaneous matching of full-scale values of parameters such as advancing tip Mach number, advance ratio, and Reynolds number. Because of these limitations, a testing medium is desired that would allow testing at model scale while matching as many of the full-scale flight parameters as possible. Freon-12 is one possibility because of its high density and low speed of sound (ref. 1). These characteristics not only aid the matching of full-scale flight parameters at model scale but also ease some restrictions on model design.

Investigations have been conducted in the past to determine the suitability of Freon-12 as a wind-tunnel test medium (refs. 1 to 6). The results generally show good correlation between air and Freon-12 data. The principal difficulty associated with using Freon-12 as

*Langley Directorate, U.S. Army Air Mobility R&D Laboratory.

a wind-tunnel test medium is the difference in the ratio of specific heats for air and Freon-12 which results in differences between the compressibility relations for the two mediums. These differences have been shown to be small for Mach numbers less than 1.4 (ref. 2).

In order to assess the use of Freon-12 as a wind-tunnel test medium for helicopter rotors, a test was conducted in the Langley transonic dynamics tunnel using Freon-12 as the test medium. A $\frac{1}{5}$-scale model dynamically similar to the standard full-scale helicopter rotor of reference 7 was tested at advancing tip Mach numbers from 0.79 to 0.95 and advance ratios from 0.3 to 0.4. Tests were also conducted at a tip-path plane angle of 0° and at full-scale Reynolds numbers using wider-chord model rotor blades. All test data obtained were compared with the full-scale data obtained in air at the same test conditions (ref. 7) to determine the degree of correlation between the two test mediums. In addition, data from the present test and those of reference 7 were compared with calculations from a helicopter rotor performance computer program based on blade-element theory.

SYMBOLS

The positive directions of forces and angles are shown in figure 1.

a blade-section lift-curve slope, rad^{-1}

a_o rotor-blade coning angle, rad

a_1 coefficient of $\cos \psi$ term in flapping-angle equation with respect to control axis

B blade tip-loss factor

b number of blades

b_1 coefficient of $\sin \psi$ term in flapping-angle equation with respect to control axis

C_D rotor drag coefficient, $\frac{D}{\rho \pi R^2 (\Omega R)^2}$

C_H rotor H-force coefficient, $\frac{H}{\rho \pi R^2 (\Omega R)^2}$

C_L rotor lift coefficient, $\frac{L}{\rho \pi R^2 (\Omega R)^2}$

$\bar{C}_L$ average blade-section lift coefficient

C_P rotor power coefficient, $\frac{P}{\rho\pi R^2(\Omega R)^3}$

C_{P_i} rotor induced-power coefficient, $\frac{P_i}{\rho\pi R^2(\Omega R)^3}$

C_{P_o} rotor profile power coefficient, $\frac{P_o}{\rho\pi R^2(\Omega R)^3}$

C_Q rotor torque coefficient, $\frac{Q}{\rho\pi R^3(\Omega R)^2}$

C_T rotor thrust coefficient, $\frac{T}{\rho\pi R^2(\Omega R)^2}$

c blade chord, cm

$\bar{c}$ speed of sound, m/sec

D rotor drag, N

g gravitational acceleration, m/sec^2

H component of rotor resultant force perpendicular to control axis in longitudinal plane, N

I_f blade mass moment of inertia about flapping axis, $N\text{-}sec^2\text{-}m$

L rotor lift, N

$M_{(1.0, 90)}$ rotor blade-tip Mach number at 90^o rotor azimuth

P rotor shaft power, N-m/sec

p pressure, N/m^2

Q rotor shaft torque, N-m

R rotor radius, m

$\bar{R}$ gas constant, $m^2/sec^2\text{-}^oK$

r	spanwise distance along blade radius measured from center of rotation, m
T	rotor thrust, N
$\bar{T}$	temperature, ^{o}K
V	free-stream velocity, m/sec
v	induced inflow velocity at rotor, m/sec
x	nondimensional spanwise distance along blade radius measured from center of rotation, r/R
$\bar{\alpha}$	average blade-section angle of attack, rad
α_c	control-axis angle of attack, deg
α_{TPP}	rotor tip-path plane angle of attack, deg
γ	ratio of specific heats
δ	section profile-drag coefficient
$\delta_1,\delta_2,\delta_3$	coefficients in power series expressing section profile-drag coefficient as function of $\bar{\alpha}$
θ	rotor-blade root (0.097R) collective pitch angle, deg
λ	rotor inflow ratio, $\left(V \sin \alpha_c - v\right)/\Omega R$
μ	rotor tip-speed ratio, $V/\Omega R$
$\bar{\mu}$	coefficient of viscosity, N-sec/m^2
ρ	mass density, kg/m^3
σ	rotor solidity, $bc/\pi R$
ψ	rotor-blade azimuth angle, rad

Ω rotor rotational speed, rad/sec

ω blade structural frequency, rad/sec

Subscripts:

i induced

o profile

p parasite

APPARATUS AND TESTS

Model Description

The model used in this investigation is shown in figures 2 and 3. The fuselage was an aerodynamic fairing of tear-drop shape and circular cross section with a fixed-incidence horizontal tail installed to minimize fuselage pitching moment. There was no vertical tail or tail rotor installed on the model.

Two model rotors were tested during this investigation. Both rotors were 292.6 cm in diameter, used an NACA 0012 airfoil section, and had -10.9° of linear twist measured from the rotor center of rotation to the rotor tip. One of the rotors was a $\frac{1}{5}$-scale representation of the full-scale standard two-bladed teetering rotor tested in reference 7 and had a chord of 10.8 cm. This rotor was dynamically scaled to have the same nondimensional structural frequencies, on a per revolution basis, as the full-scale rotor of reference 7. The factors required to maintain dynamic similarity of the $\frac{1}{5}$-scale rotor in freon are presented in table I. The second rotor was used for the full-scale Reynolds number testing and had a chord of 25.4 cm. This rotor was not dynamically scaled, and its structural stiffnesses were an order of magnitude greater than those of the $\frac{1}{5}$-scale rotor. The rotors were powered by two 35-kilowatt electric motors located in the fuselage. The rotors were remotely controlled through a conventional swashplate system that provided blade collective pitch as well as longitudinal and lateral cyclic pitch.

The entire model, including the model pitch mechanism, was attached to a six-component strain-gage balance. This model/balance assembly was mounted in the tunnel so that the rotor disk plane was approximately on the tunnel center line.

Instrumentation

Instrumentation provided model forces and moments, rotor-blade loads, rotor rotational speed (rpm), and model-position data. Total model (rotor and fuselage) forces and moments were measured by the six-component strain-gage balance on which the model was mounted. Main-rotor torque was measured by a strain-gage bridge mounted on the main-rotor shaft. Blade bending moments were also measured by strain-gage bridges at the 15.6, 28.8, 47.9, and 59.0 percent blade-radius stations. Rotor-blade collective pitch as well as longitudinal and lateral cyclic pitch, model-pitch attitude, rotor flapping, and rotor rotational speed were measured and displayed at the model control panel.

All tunnel-condition data, model-balance data, shaft torque, control positions, and rotor rotational speed were recorded on the tunnel data-acquisition system.

The accuracies of the data have been estimated to be within the following limits:

C_L	±0.00017
C_D	±0.00011
C_Q	±0.000033
Shaft angle of attack, collective pitch, lateral and longitudinal cyclic pitch, deg	±0.25

Test Procedure

The purpose of this test was to obtain aerodynamic data for a model helicopter rotor system operating in a Freon-12 atmosphere.

In order to obtain "rotor only" aerodynamic forces and moments, model static and dynamic tares were determined and applied to the data. Model static tares were determined by recording data throughout the model-pitch range (wind off) for both the rotor-on and rotor-off configurations. Model dynamic tares (wind on) were determined throughout the model-pitch range at three values of tunnel dynamic pressure and two values of shaft rotational speed for the model with the rotor off. The model dynamic tares were found to be a function of model-pitch attitude and tunnel dynamic pressure. They were not affected by shaft rotational speed for the values tested.

For each test point, the rotor rotational speed and tunnel conditions were adjusted to give the desired values of advancing tip Mach number and advance ratio. The model was then pitched to the desired shaft angle. Blade collective pitch was changed to obtain a variation in rotor lift, and cyclic pitch was used to remove rotor first-harmonic flapping with respect to the rotor shaft. Data were then recorded at each value of collective pitch. The maximum value of collective pitch attained was determined in most cases by blade load limits.

PRESENTATION OF RESULTS

The results in this report are presented in figures as follows:

	Figure
Measured rotor characteristics	4 to 6
Comparison of calculated and measured rotor performance	7 to 9
Effect of scaling parameters on rotor performance	10 to 13

DISCUSSION OF RESULTS

Measured Rotor Characteristics

The $\frac{1}{5}$-scale model rotor data obtained in a freon atmosphere during this investigation and full-scale rotor data obtained in air (ref. 7) are presented in figures 4 to 6. The constant collective pitch lines shown in figure 4 for the freon data are nominal values, and lines of constant collective pitch are omitted from figures 5 and 6 for clarity.

The correlation between model and full-scale results, with regard to data trends, is shown (figs. 4 to 6) to be good throughout the range of μ and $M_{(1.0,\ 90)}$ tested. However, differences in θ and α_c between model and full-scale results can be seen in figure 4 for a given C_L/σ and α_{TPP}. As μ and $M_{(1.0,\ 90)}$ are increased, the differences in α_c are minimized while the model continues to require higher values of θ. Figure 5 shows that, for a given C_L/σ and α_{TPP}, the quality of the agreement of full-scale and model-scale values of C_D/σ varies with μ and $M_{(1.0,\ 90)}$. Figure 6 shows the model requires higher than full-scale values of C_Q/σ for all test conditions.

Comparison of Calculated and Measured Rotor Performance

Rotor performance data obtained during this test and that of reference 7 are compared in figures 7 to 9 with calculations from a general rotor performance computer program. The equations programed are those of reference 8. The program utilizes a rigid blade with pitch and flap degrees of freedom. No lag motion is provided, and rotor inflow is assumed constant over the disk. The rotor-blade airfoil characteristics vary with both angle of attack and Mach number. The airfoil data used are those of reference 9.

Figure 7 shows good correlation of model and full-scale values of C_Q/σ for fixed values of C_L/σ and C_D/σ, except at $\mu = 0.40$ (fig. 7(e)). The theoretical results generally correlate with the full-scale results at least as well as, or better than, model results at all values of μ and $M_{(1.0,\ 90)}$ tested. The airfoil data used in the theory are based on full-scale Reynolds number, and this fact may account for the degree of correlation between theoretical and full-scale results, particularly at $\mu = 0.40$.

Figures 8 and 9 are cross plotted from figure 7 to show the effects of $M_{(1.0,\ 90)}$ and μ on C_Q/σ for fixed values of C_L/σ and C_D/σ. Figure 8 shows the expected increase in C_Q/σ due to compressibility as $M_{(1.0,\ 90)}$ is increased at constant μ. The correlation between the model data and full-scale data is generally good over the range of $M_{(1.0,\ 90)}$ tested, with the best correlation occurring at the highest value of $M_{(1.0,\ 90)}$. The prediction of full-scale data using theoretical results at the highest $M_{(1.0,\ 90)}$ in figure 8 is inconsistent. The theory underpredicts C_Q/σ at the lower values of C_L/σ (figs. 8(a) and 8(b)) and overpredicts at the higher value of C_L/σ (fig. 8(c)). This inconsistent correlation in C_Q/σ, which seems to be a function of lift coefficient, may be due in part to the theoretical modeling of lift-curve slope as a function of Mach number. If this modeling is not done precisely, a section lift coefficient will be analytically predicted to occur at a different angle of attack, which will produce a different section drag coefficient and result in a different value of C_Q/σ from that experienced by full-scale rotors.

Figure 9 shows the effect of μ on C_Q/σ for a fixed $M_{(1.0,\ 90)}$. As μ is increased beyond a value of 0.35, the model data begin to deviate significantly from full-scale values. As μ is increased to 0.40, low total velocity on the retreating blade may, through Reynolds number effects, cause high values of C_Q/σ which full-scale hardware does not experience and theoretical results do not predict.

Effect of Scaling Parameters on Rotor Performance

Figures 10 to 13 show the effects of Reynolds number, rotor solidity, and blade elasticity on rotor performance. Reynolds number was determined using the rotor-blade chord and total velocity at the blade tip at a rotor azimuth of 90°. Data are presented in figure 10 for the 25.4 cm chord model rotor at various values of Reynolds number. This variation in Reynolds number was accomplished by adjusting the tunnel parameters to change the density of the test medium. Comparison of these data shows a measurable effect on rotor performance for a large change in Reynolds number. Data are also presented in figure 10 for the full-scale rotor of reference 7 and the $\frac{1}{5}$-scale model rotor at Reynolds numbers corresponding to the test condition of $\mu = 0.30$, $M_{(1.0,\ 90)} = 0.85$ for each rotor. Comparison of these data shows the relatively small effect of Reynolds number on the performance of two rotors with the same solidity and dynamic characteristics. Comparison of the 25.4 cm chord model rotor data at the same two values of Reynolds number as the full-scale rotor and the $\frac{1}{5}$-scale model rotor also shows a small effect of Reynolds number on rotor performance. Comparing the 25.4 cm chord model rotor data with either the full-scale rotor data or the $\frac{1}{5}$-scale model rotor data, at their respective Reynolds numbers, shows a significant effect of rotor solidity and blade elasticity on rotor performance.

Figures 11 and 12 show data for the full-scale rotor of reference 7, the $\frac{1}{5}$-scale model rotor in freon at model-scale values of Reynolds number, and the 25.4 cm chord model rotor operating in freon at full-scale values of Reynolds number. In order to compare the performance of each rotor more directly, solidity corrections similar to those of reference 9 were made to the 25.4 cm chord rotor data. These corrections are described in the appendix. Figures 11 and 12 show that the $\frac{1}{5}$-scale model rotor data generally correlate better with the full-scale rotor data than the corrected full-scale Reynolds number data from the 25.4 cm chord model rotor. These data tend to substantiate the conclusions of figure 10 with respect to Reynolds number effects.

The data in figures 11 and 12 also show the effect of differences in blade elasticity on rotor performance. The $\frac{1}{5}$-scale model rotor was a dynamically scaled version of the full-scale rotor but did not operate at full-scale values of Reynolds number. The 25.4 cm chord model rotor was not dynamically scaled but did operate at full-scale values of Reynolds number. The degree of correlation shown in figures 11 and 12 between the model rotors and the full-scale rotor, in addition to the results of figure 10, shows that the importance of matching full-scale values of Reynolds number for rotor performance testing does not appear to be as great as the need to match rotor solidity and blade elastic properties.

In figure 13, the effects of $M_{(1.0,\ 90)}$ and μ are shown for both full-scale and $\frac{1}{5}$-scale model values of Reynolds number. For the range of $M_{(1.0,\ 90)}$ tested, the correlation between full-scale Reynolds number data in both air and freon is seen to improve as $M_{(1.0,\ 90)}$ increases above a value of 0.85. For the range of μ tested, the correlation between the $\frac{1}{5}$-scale model Reynolds number data and full-scale Reynolds number data is not significantly affected by increasing μ.

CONCLUSIONS

An investigation has been conducted in the Langley transonic dynamics tunnel to determine the degree of correlation between model-scale helicopter rotor performance data obtained in a freon atmosphere and full-scale helicopter rotor performance data obtained in air. Based on the data obtained, the following conclusions have been reached:

1. Correlation of model-scale rotor performance data in freon with full-scale rotor performance data in air is good with regard to data trends.

2. Mach number effects on model rotor performance data obtained in freon are essentially the same as for full-scale rotor aerodynamic performance data obtained in air.

3. Reynolds number effects may be minor in rotor aerodynamic performance testing in comparison to the combined effects of rotor solidity and blade elastic properties.

4. Rotor solidity has a significant effect on rotor C_D/σ and C_Q/σ for a fixed value of α_{TPP}.

5. Blade elastic modeling should be considered a significant parameter in model rotor aerodynamic performance testing.

Langley Research Center
National Aeronautics and Space Administration
Hampton, VA 23665
October 1, 1976

APPENDIX

DERIVATION OF SOLIDITY CORRECTION FACTORS

Reference 9 has derived solidity corrections for C_D/σ for given values of λ, θ, and μ. The solidity corrections used in this paper for C_P/σ and C_D/σ are derived for fixed values of C_L/σ, α_{TPP}, and μ but allow for changes in λ and θ with changes in rotor solidity.

The expression for rotor power coefficient may be written as follows:

$$C_P = C_Q = C_{P_o} + C_{P_i} + C_{P_p} \qquad \text{(ref. 10)} \qquad (1)$$

where

$$C_{P_o} = \frac{\sigma\delta}{8}\left(1 + 3\mu^2\right) \qquad \text{(ref. 11)} \qquad (2)$$

$$C_{P_i} = \frac{\left(C_L/\sigma\right)^2}{2\mu}\,\sigma^2 \qquad \text{(ref. 10)} \qquad (3)$$

and

$$C_{P_p} = -C_D\mu \qquad \text{(ref. 10)} \qquad (4)$$

assuming $C_T = C_L$ and α_c is small.

Equations 1 to 4 result in the following:

$$C_P = \frac{\sigma\delta}{8}\left(1 + 3\mu^2\right) + \frac{\left(C_L/\sigma\right)^2}{2\mu}\,\sigma^2 - C_D\mu \qquad (5)$$

The rotor power coefficient/solidity ratio is, from equation (5),

$$\frac{C_P}{\sigma} = \frac{\delta}{8}\left(1 + 3\mu^2\right) + \frac{\left(C_L/\sigma\right)^2}{2\mu}\,\sigma - \left(\frac{C_D}{\sigma}\right)\mu \qquad (6)$$

and the change in rotor power coefficient/solidity ratio due to a change in solidity is, from equation (6),

$$\frac{\partial\left(C_P/\sigma\right)}{\partial\sigma} = \left(\frac{1 + 3\mu^2}{8}\right)\frac{\partial\delta}{\partial\sigma} + \frac{\left(C_L/\sigma\right)^2}{2\mu} - \mu\,\frac{\partial\left(C_D/\sigma\right)}{\partial\sigma} \qquad (7)$$

APPENDIX

An expression for blade-section mean lift coefficient in forward flight may be determined from the following:

$$C_T = \frac{\bar{C}_L \sigma}{2} \frac{1}{2\pi} \int_0^{2\pi} \int_0^B \left(x^2 + 2x\mu \sin \psi + \mu^2 \sin^2 \psi\right) dx\, d\psi \tag{8}$$

Performing the indicated integration and assuming $C_T = C_L$ gives

$$\bar{C}_L = \frac{6\left(C_L/\sigma\right)}{B^3 + \frac{3}{2} B\mu^2} = a\bar{\alpha} \tag{9}$$

An expression for rotor blade-section profile drag coefficient may be written as follows:

$$\delta = \delta_1 + \delta_2 \bar{\alpha} + \delta_3 \bar{\alpha}^2 \tag{10}$$

Combining equations (9) and (10) gives

$$\delta = \delta_1 + \delta_2 \left(\frac{\bar{C}_L}{a}\right) + \delta_3 \left(\frac{\bar{C}_L}{a}\right)^2 \tag{11}$$

If Reynolds number effects are assumed small, then δ_1, δ_2, δ_3, and a can be assumed constant and equation (11) gives

$$\frac{\partial \delta}{\partial \sigma} = \frac{\delta_2}{a} \frac{\partial \bar{C}_L}{\partial \sigma} + \frac{2\delta_3}{a^2} \bar{C}_L \frac{\partial \bar{C}_L}{\partial \sigma} \tag{12}$$

If C_L/σ is maintained constant, then equations (9) and (12) will give

$$\frac{\partial \delta}{\partial \sigma} = 0 \tag{13}$$

Combining equations (7) and (13) gives

$$\frac{\partial\left(C_P/\sigma\right)}{\partial \sigma} = \frac{\left(C_L/\sigma\right)^2}{2\mu} - \mu \frac{\partial\left(C_D/\sigma\right)}{\partial \sigma} \tag{14}$$

The rotor drag/solidity ratio may be written as follows:

$$\frac{C_D}{\sigma} = \frac{C_T}{\sigma} \sin \alpha_c + \frac{C_H}{\sigma} \cos \alpha_c \tag{15}$$

The change in rotor drag coefficient/solidity ratio due to a change in solidity is:

APPENDIX

$$\frac{\partial\left(C_D/\sigma\right)}{\partial\sigma} = \frac{C_T}{\sigma}\cos\alpha_c\frac{\partial\alpha_c}{\partial\sigma} + \sin\alpha_c\frac{\partial\left(C_T/\sigma\right)}{\partial\sigma} + \cos\alpha_c\frac{\partial\left(C_H/\sigma\right)}{\partial\sigma}$$

$$-\frac{C_H}{\sigma}\sin\alpha_c\frac{\partial\alpha_c}{\partial\sigma} \tag{16}$$

Making the assumptions that $\frac{C_T}{\sigma} = \frac{C_L}{\sigma}$, $\frac{C_L}{\sigma}$ is maintained constant, α_c is small, and $\frac{C_H}{\sigma} \ll \frac{C_L}{\sigma}$, equation (16) becomes

$$\frac{\partial\left(C_D/\sigma\right)}{\partial\sigma} = \frac{C_L}{\sigma}\frac{\partial\alpha_c}{\partial\sigma} + \frac{\partial\left(C_H/\sigma\right)}{\partial\sigma} \tag{17}$$

Then, if $\lambda \ll \mu$ and $\alpha_{TPP} = 0^o$, an expression for α_c may be written as follows (ref. 12):

$$\alpha_c = \frac{\lambda}{\mu} + \frac{\left(C_L/\sigma\right)}{2\mu^2}\sigma = -a_1 \tag{18}$$

and then,

$$\frac{\partial\alpha_c}{\partial\sigma} = \frac{1}{\mu}\frac{\partial\lambda}{\partial\sigma} + \frac{\left(C_L/\sigma\right)}{2\mu^2} = -\frac{\partial a_1}{\partial\sigma} \tag{19}$$

Using the equations of reference 12, expressions for $\frac{\partial\theta}{\partial\sigma}$ and $\frac{\partial\lambda}{\partial\sigma}$ can be determined as

$$\frac{\partial\theta}{\partial\sigma} = \frac{-1}{\frac{2}{3} + \mu^2}\frac{\partial\lambda}{\partial\sigma} \tag{20}$$

$$\frac{\partial\lambda}{\partial\sigma} = \frac{-\left(1 + \mu^2\right)}{2\mu\left(1 - \mu^2\right)}\frac{C_L}{\sigma} \tag{21}$$

An expression for a_1 may be written as follows (ref. 12):

$$a_1 = \frac{2\mu}{1 - \frac{1}{2}\mu^2}\left(\frac{4}{3}\theta + \lambda\right) \tag{22}$$

and then,

$$\frac{\partial a_1}{\partial\sigma} = \frac{2\mu}{1 - \frac{1}{2}\mu^2}\left(\frac{4}{3}\frac{\partial\theta}{\partial\sigma} + \frac{\partial\lambda}{\partial\sigma}\right) \tag{23}$$

APPENDIX

Substitution of equations (20) and (21) into equation (23) gives

$$\frac{\partial a_1}{\partial \sigma} = \left(1 - \frac{\mu^2}{2}\right)\frac{C_L}{\sigma} \tag{24}$$

Substitution of equation (24) into equation (19) gives

$$\frac{\partial \alpha_c}{\partial \sigma} = -\left(1 - \frac{\mu^2}{2}\right)\frac{C_L}{\sigma} \tag{25}$$

and equation (17) then becomes

$$\frac{\partial\left(C_D/\sigma\right)}{\partial \sigma} = -\left(1 - \frac{\mu^2}{2}\right)\left(\frac{C_L}{\sigma}\right)^2 + \frac{\partial\left(C_H/\sigma\right)}{\partial \sigma} \tag{26}$$

An expression for C_H/σ may be written as follows (ref. 12):

$$\frac{C_H}{\sigma} = \frac{a}{2}\left(\frac{\delta\mu}{2a} + \frac{\theta a_1}{3} - \frac{\mu\lambda\theta}{2} + \frac{3\lambda a_1}{4} + \frac{\mu a_1^2}{4} - \frac{a_o b_1}{6} + \frac{\mu a_o^2}{4}\right) \tag{27}$$

The change in C_H/σ due to a change in rotor solidity is then

$$\frac{\partial\left(C_H/\sigma\right)}{\partial \sigma} = \frac{a}{2}\left(\frac{\mu}{2a}\frac{\partial \delta}{\partial \sigma} + \frac{\theta}{3}\frac{\partial a_1}{\partial \sigma} + \frac{a_1}{3}\frac{\partial \theta}{\partial \sigma} - \frac{\mu\lambda}{2}\frac{\partial \theta}{\partial \sigma} - \frac{\mu\theta}{2}\frac{\partial \lambda}{\partial \sigma}\right.$$

$$\left. + \frac{3\lambda}{4}\frac{\partial a_1}{\partial \sigma} + \frac{3a_1}{4}\frac{\partial \lambda}{\partial \sigma} + \frac{\mu a_1}{2}\frac{\partial a_1}{\partial \sigma} - \frac{a_o}{6}\frac{\partial b_1}{\partial \sigma} - \frac{b_1}{6}\frac{\partial a_o}{\partial \sigma} + \frac{\mu a_o}{2}\frac{\partial a_o}{\partial \sigma}\right) \tag{28}$$

Since, for a teetering rotor, a_o is a constant equal to the precone angle and making use of equation (13), equation (28) becomes

$$\frac{\partial\left(C_H/\sigma\right)}{\partial \sigma} = \frac{a}{2}\left[\left(\frac{\theta}{3} + \frac{3\lambda}{4} + \frac{\mu a_1}{2}\right)\frac{\partial a_1}{\partial \sigma} + \left(\frac{a_1}{3} - \frac{\mu\lambda}{2}\right)\frac{\partial \theta}{\partial \sigma} + \left(\frac{3a_1}{4} - \frac{\mu\theta}{2}\right)\frac{\partial \lambda}{\partial \sigma}\right] \tag{29}$$

Combining equations (20), (21), (23), and (29), equation (26) becomes

$$\frac{\partial\left(C_D/\sigma\right)}{\partial \sigma} = \left(1 - \frac{\mu^2}{2}\right)\frac{C_L}{\sigma}\left\{-\frac{C_L}{\sigma} + \frac{a}{4}\left(\frac{2\theta}{3} + \frac{3\lambda}{2} + \mu a_1\right)\right.$$

$$\left. + \frac{a}{4}\left(\frac{2a_1}{3} - \mu\lambda\right)\left[\frac{3\left(1 + \mu^2\right)}{4\mu}\right] - \frac{a}{4}\left(\frac{3a_1}{2} - \mu\theta\right)\left(\frac{1 + \mu^2}{2\mu - 3\mu^3}\right)\right\} \tag{30}$$

APPENDIX

The values of C_P/σ and C_D/σ corrected for changes in rotor solidity may then be determined as follows from equations (14) and (30), respectively, as follows:

$$\left(C_P/\sigma\right)_{desired} = \left(C_P/\sigma\right)_{actual} + \frac{\partial\left(C_P/\sigma\right)}{\partial\sigma}\left(\sigma_{desired} - \sigma_{actual}\right) \tag{31}$$

$$\left(C_D/\sigma\right)_{desired} = \left(C_D/\sigma\right)_{actual} + \frac{\partial\left(C_D/\sigma\right)}{\partial\sigma}\left(\sigma_{desired} - \sigma_{actual}\right) \tag{32}$$

REFERENCES

1. Von Doenhoff, Albert E.; Braslow, Albert L.; and Schwartzberg, Milton A.: Studies of the Use of Freon-12 as a Wind-Tunnel Testing Medium. NACA TN 3000, 1953.

2. Huber, Paul W.: Use of Freon-12 as a Fluid for Aerodynamic Testing. NACA TN 1024, 1946.

3. Pozniak, O. M.: Investigation Into the Use of Freon 12 as a Working Medium in a High-Speed Wind-Tunnel. Note No. 72, Coll. Aeronaut., Cranfield (Engl.), Nov. 1957.

4. Yates, E. Carson, Jr.; and Sandford, Maynard C.: Static Longitudinal Aerodynamic Characteristics of an Elastic Canard-Fuselage Configuration as Measured in Air and in Freon-12 at Mach Numbers up to 0.92. NASA TN D-1792, 1963.

5. Treon, Stuart L.; Hofstetter, William R.; and Abbott, Frank T., Jr.: On the Use of Freon-12 for Increasing Reynolds Number in Wind-Tunnel Testing of Three-Dimensional Aircraft Models at Subcritical and Supercritical Mach Numbers. Facilities and Techniques for Aerodynamic Testing at Transonic Speeds and High Reynolds Number, AGARD CP No. 83, Aug. 1971, pp. 27-1 – 27-8.

6. Lee, Charles; Charles, Bruce; and Kidd, David: Wind-Tunnel Investigation of a Quarter-Scale Two-Bladed High-Performance Rotor in a Freon Atmosphere. USAAVLABS Tech. Rep. 70-58, U.S. Army, Feb. 1971.

7. Tanner, W. H.; and Van Wyckhouse, J. F.: Wind Tunnel Tests of Full-Scale Rotors Operating at High Advancing Tip Mach Numbers and Advance Ratios. USAAVLABS Tech. Rep. 68-44, U.S. Army, July 1968. (Available from DDC as AD 674 188.)

8. Gessow, Alfred; and Crim, Almer D.: A Method for Studying the Transient Blade-Flapping Behavior of Lifting Rotors at Extreme Operating Conditions. NACA TN 3366, 1955.

9. Tanner, Watson H.: Charts for Estimating Rotary Wing Performance in Hover and at High Forward Speeds. NASA CR-114, 1964.

10. Gessow, Alfred; and Tapscott, Robert J.: Charts for Estimating Performance of High-Performance Helicopters. NACA Rep. 1266, 1956. (Supersedes NACA TN 3323 by Gessow and Tapscott and TN 3482 by Tapscott and Gessow.)

11. Gessow, Alfred: Equations and Procedures for Numerically Calculating the Aerodynamic Characteristics of Lifting Rotors. NACA TN 3747, 1956.

12. Gessow, Alfred; and Myers, Garry C., Jr.: Aerodynamics of the Helicopter. Macmillan Co., c.1952. (Republished 1967 by Frederick Ungar Pub. Co.)

TABLE I.- TYPICAL SCALING PARAMETERS FOR A $\frac{1}{5}$-SCALE MODEL IN AIR AND FREON-12 TEST MEDIUMS

Parameter	General scaling formula	[a]Scale factors	
		Air	Freon-12
Speed of sound	$\sqrt{\gamma \bar{R} \bar{T}}$	1.0	0.448
Density	$p/\bar{R}\bar{T}$	1.0	4.0
Coefficient of viscosity	$\bar{\mu}$	1.0	.705
Length	R	.2	.2
Mass	$R^3\rho$	.008	.032
Time	$R/\bar{c}$	.2	.446
Angular velocity	$\bar{c}/R$	5.0	2.24
Linear velocity	$\bar{c}$	1.0	.448
Force	$R^2\rho\bar{c}^2$	.04	.032
Moment	$R^3\rho\bar{c}^2$	.008	.0064
Power	$R^2\rho\bar{c}^3$	.04	.0143
Mach number	$V/\bar{c}$	1.0	1.0
Froude number	$\bar{c}^2/gR$	5.0	1.0
Reynolds number	$\rho VR/\bar{\mu}$	.2	.508
Advance ratio	$V/\Omega R$	1.0	1.0
Locke number	$\rho acR^4/I_f$	1.0	1.0
Structural frequencies	ω/Ω	1.0	1.0

[a]Based on full atmospheric pressure and standard day conditions. Scale factor equals ratio of model to full-scale values.

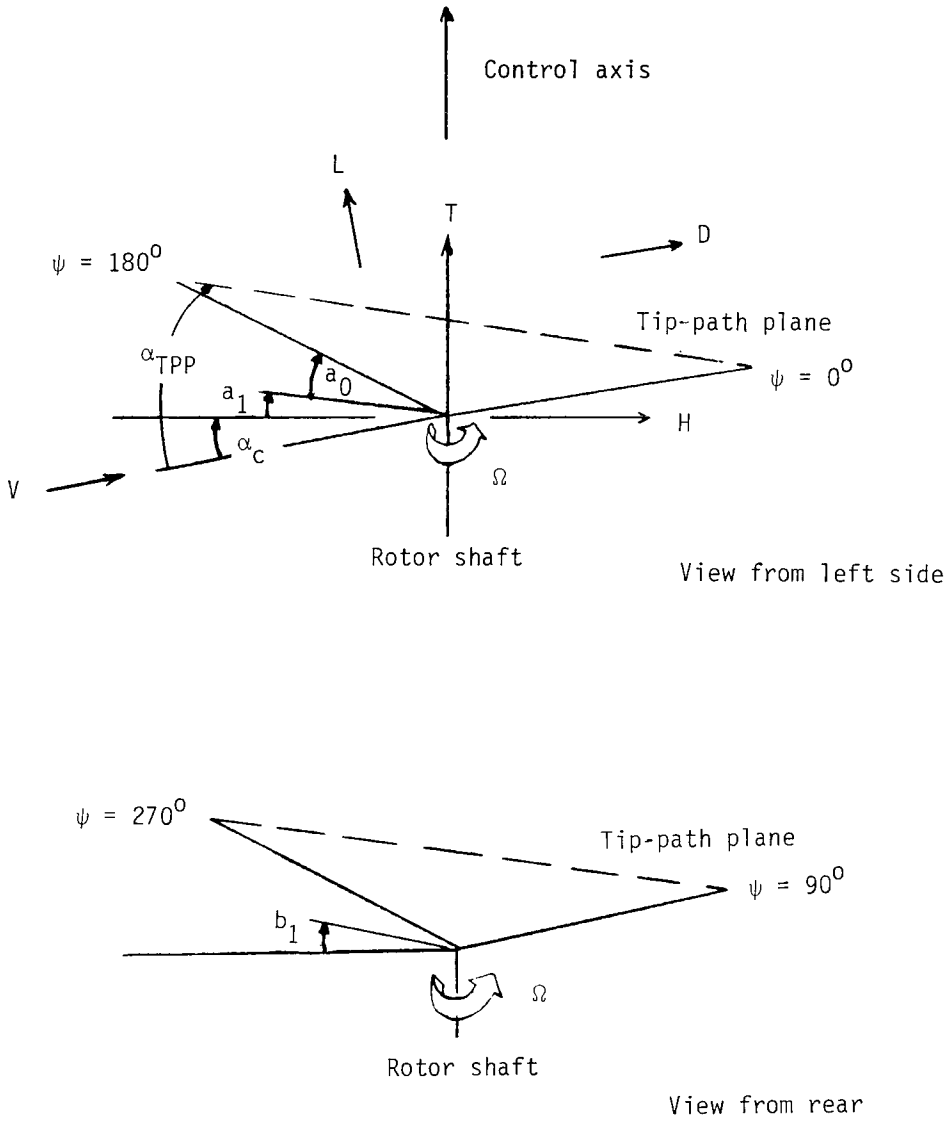

Figure 1.- Notation showing positive direction of forces and angles.

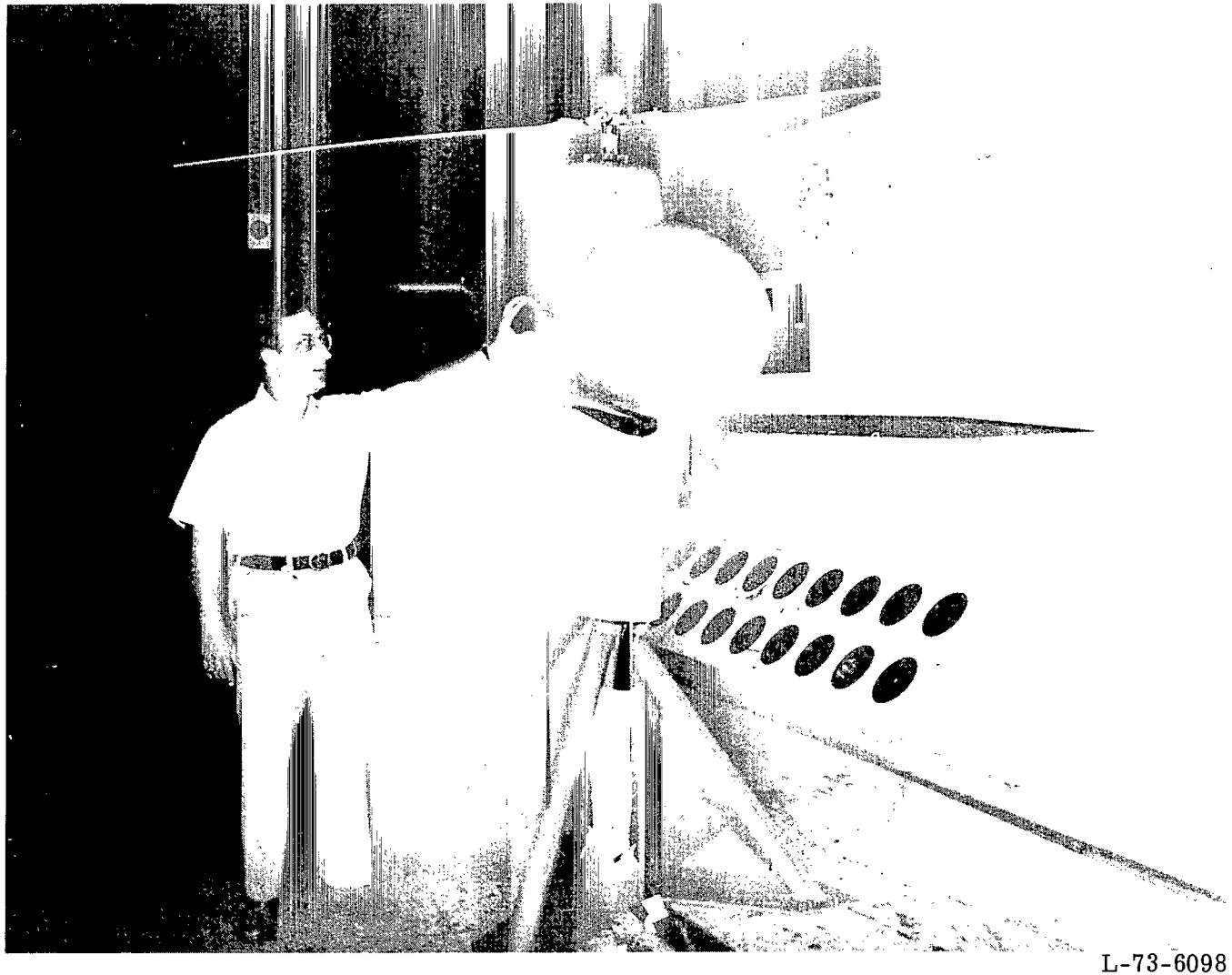

L-73-6098

Figure 2.- Model installed in Langley transonic dynamics tunnel.

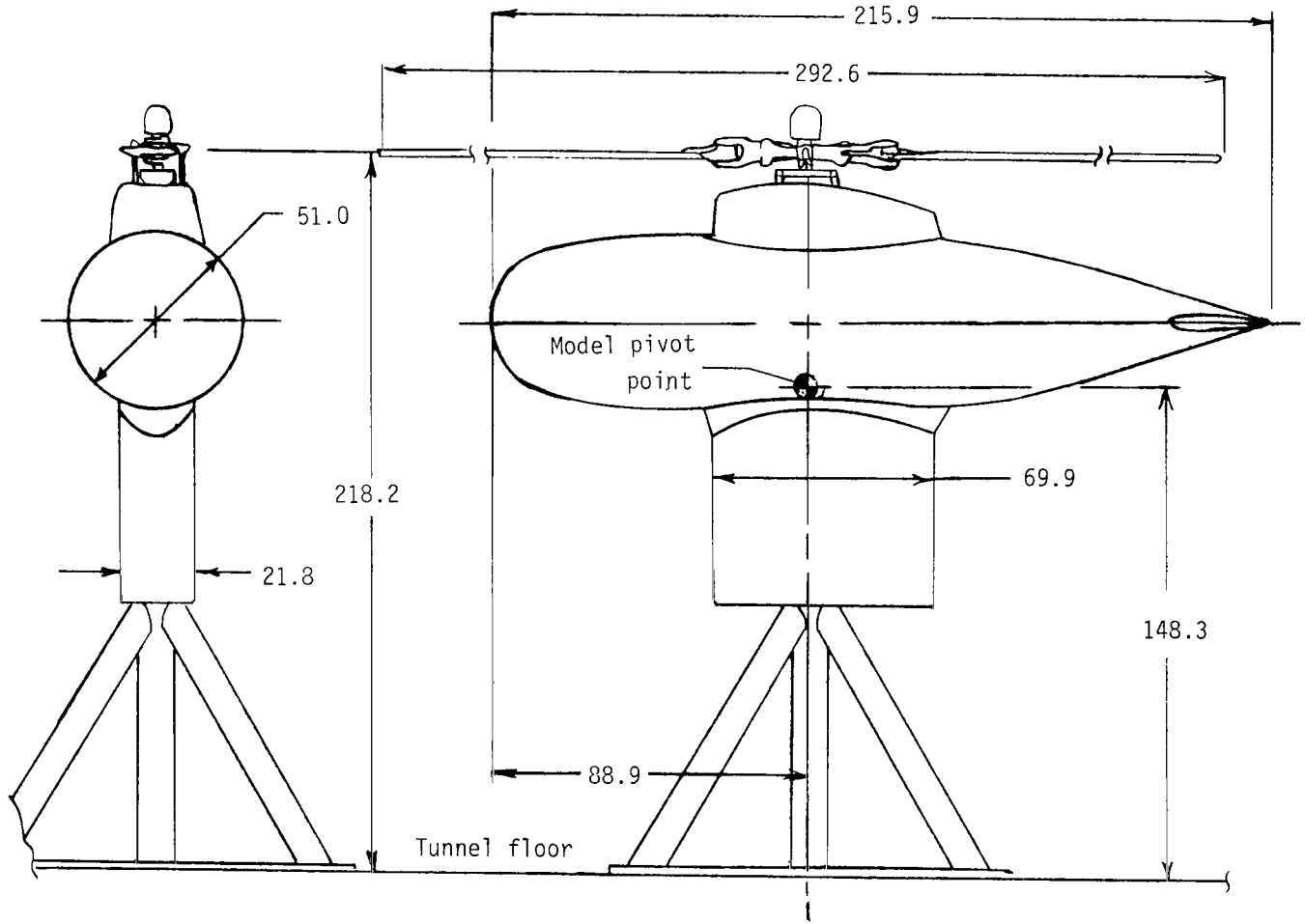

Figure 3.- Tunnel installation dimensional data. (All dimensions are in centimeters.)

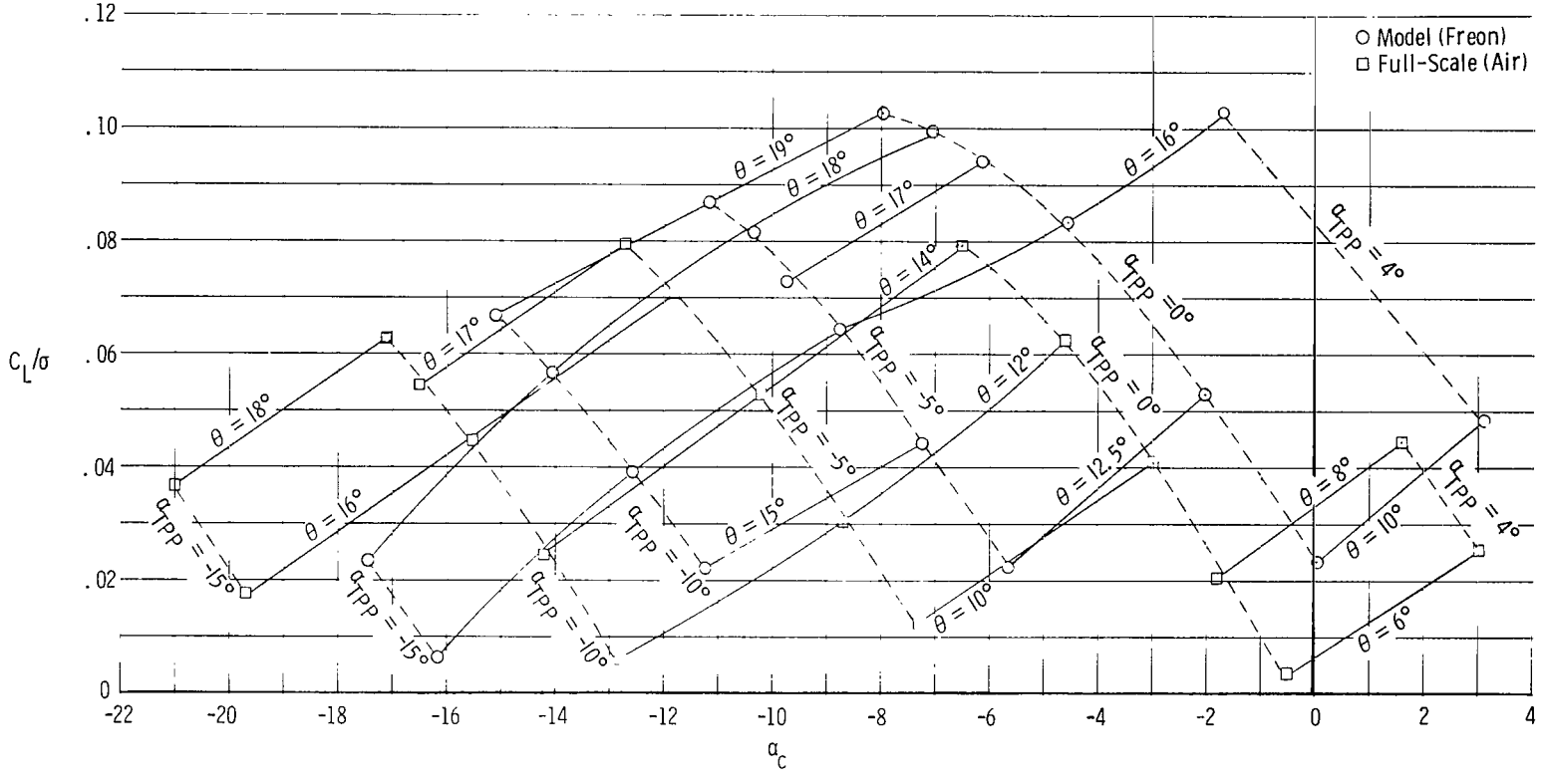

(a) $\mu = 0.30$, $M_{(1.0, 90)} = 0.79$.

Figure 4.- Comparison of freon model and full-scale performance for various control positions.

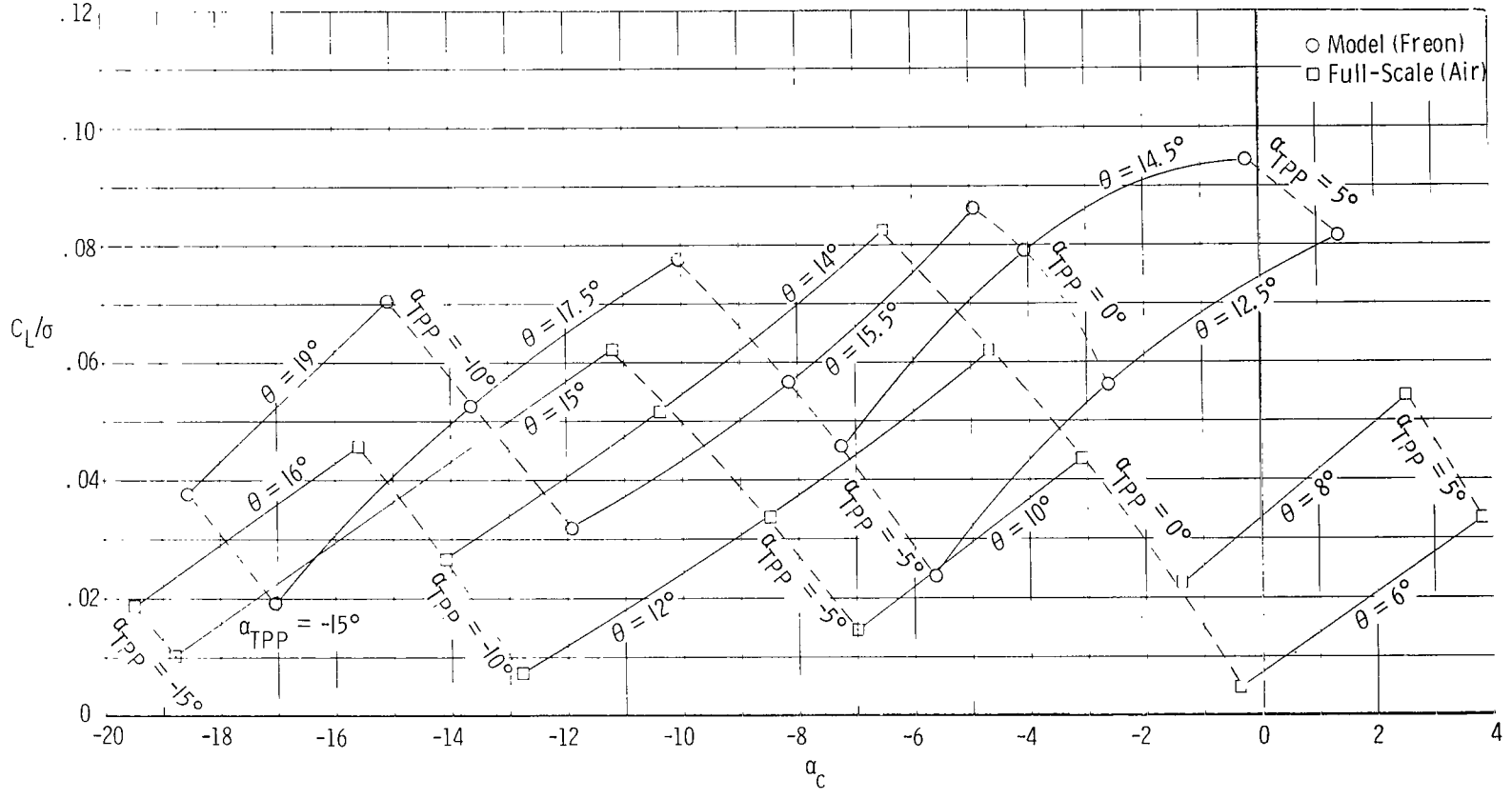

(b) $\mu = 0.30$, $M_{(1.0,\ 90)} = 0.85$.

Figure 4.- Continued.

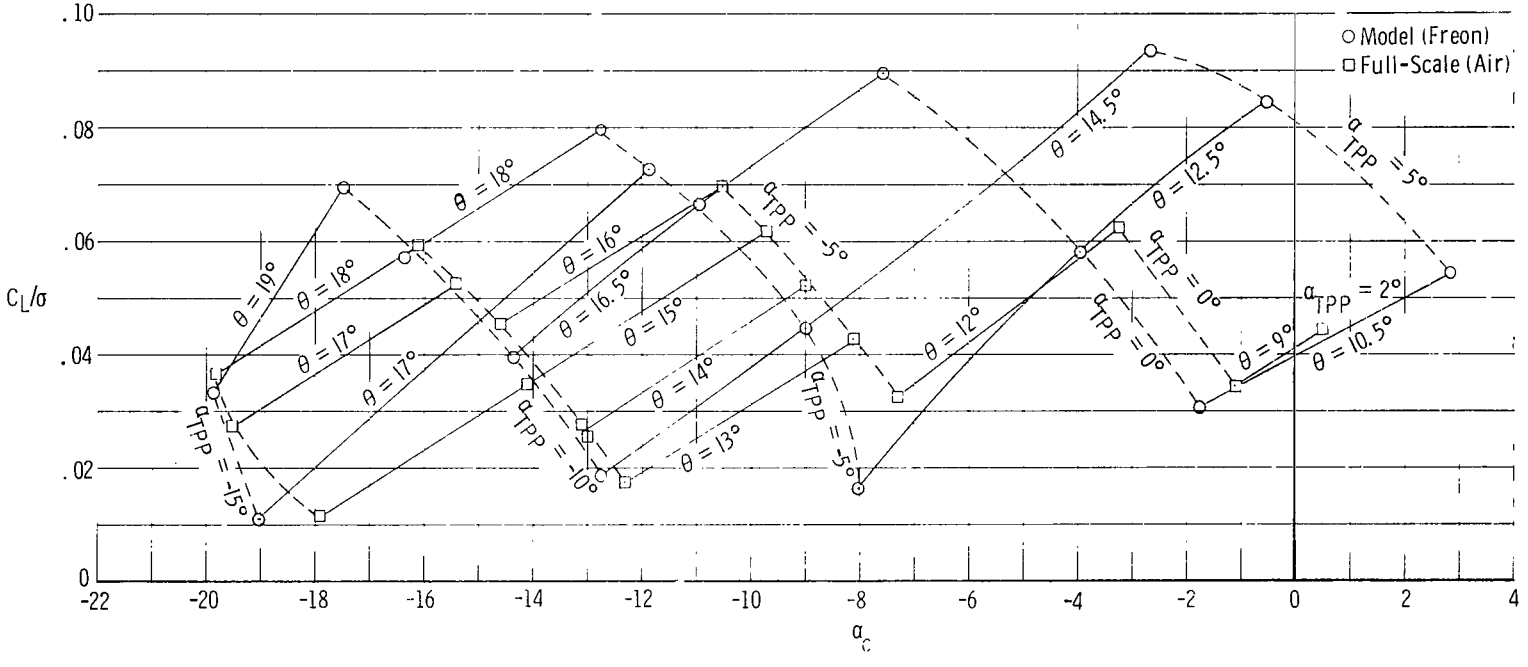

(c) $\mu = 0.30$, $M_{(1.0,\ 90)} = 0.95$.

Figure 4.- Continued.

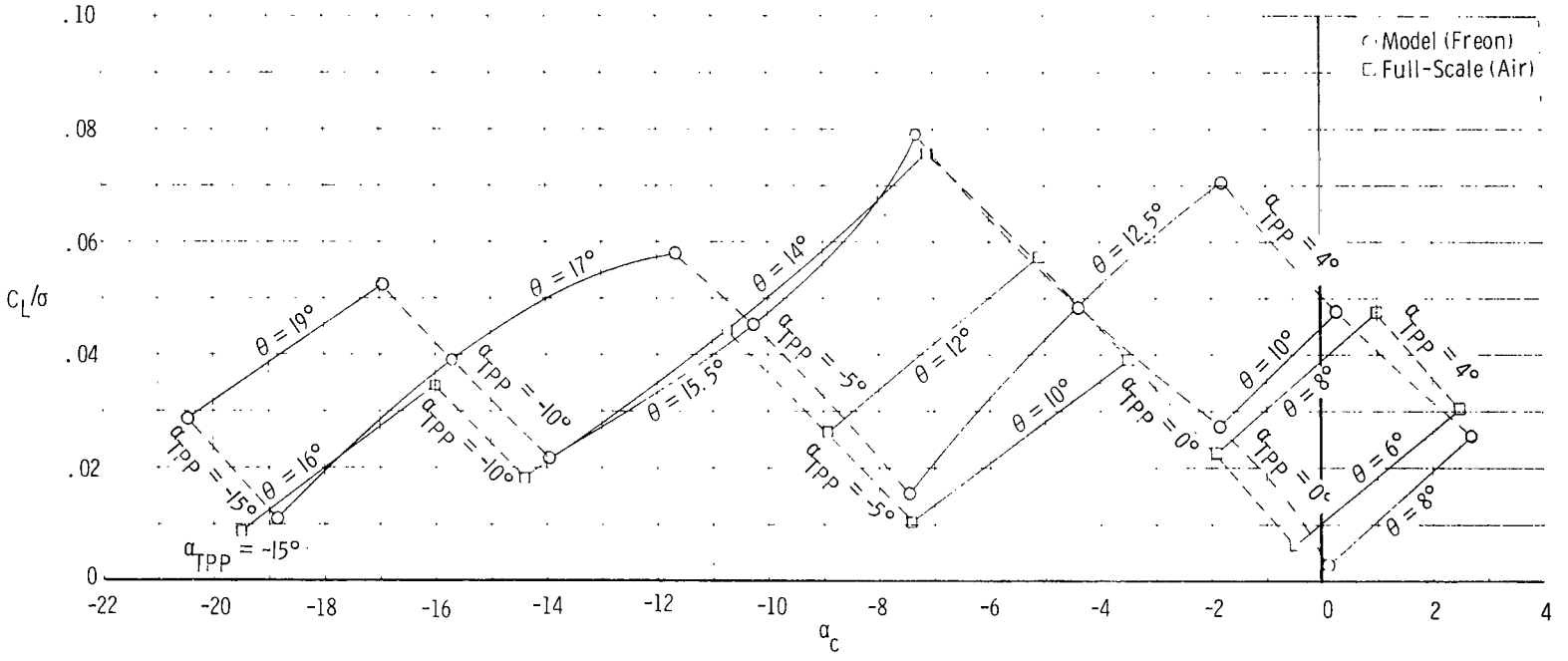

(d) $\mu = 0.35$, $M_{(1.0,\ 90)} = 0.85$.

Figure 4.- Continued.

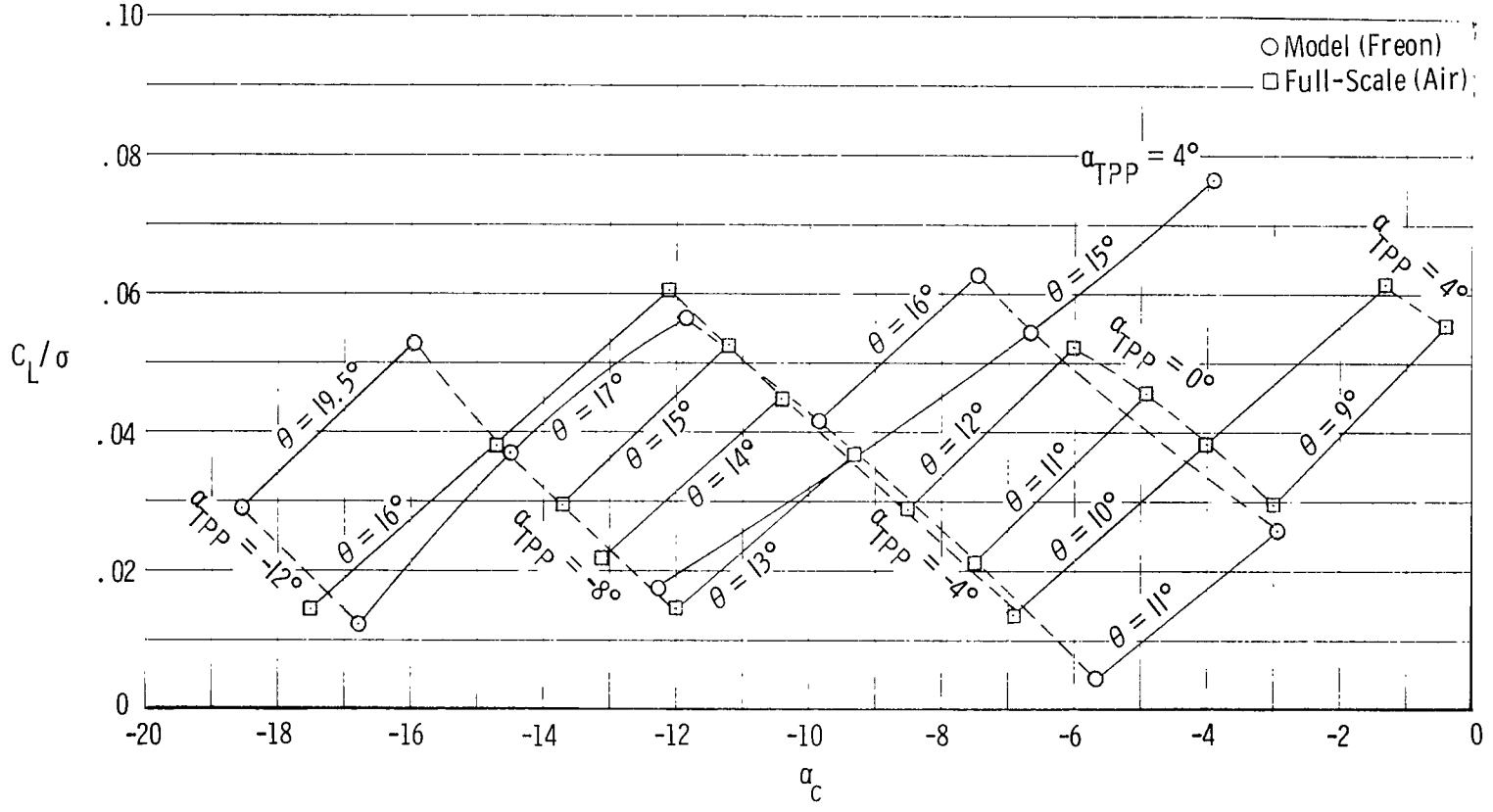

(e) $\mu = 0.40$, $M_{(1.0, 90)} = 0.85$.

Figure 4.- Concluded.

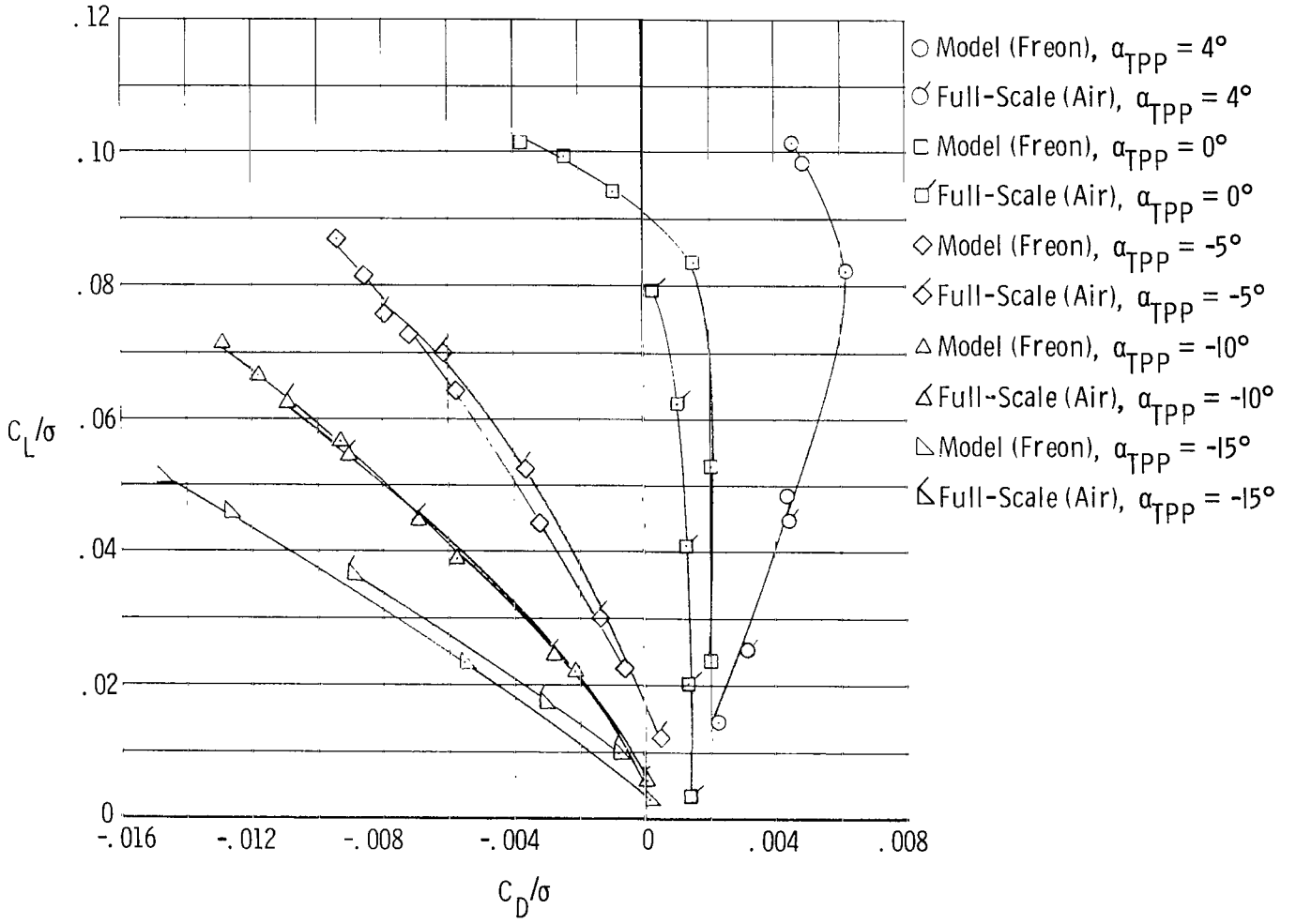

(a) $\mu = 0.30$, $M_{(1.0,\ 90)} = 0.79$.

Figure 5.- Comparison of freon model and full-scale values of C_L/σ and C_D/σ for various values of α_{TPP}.

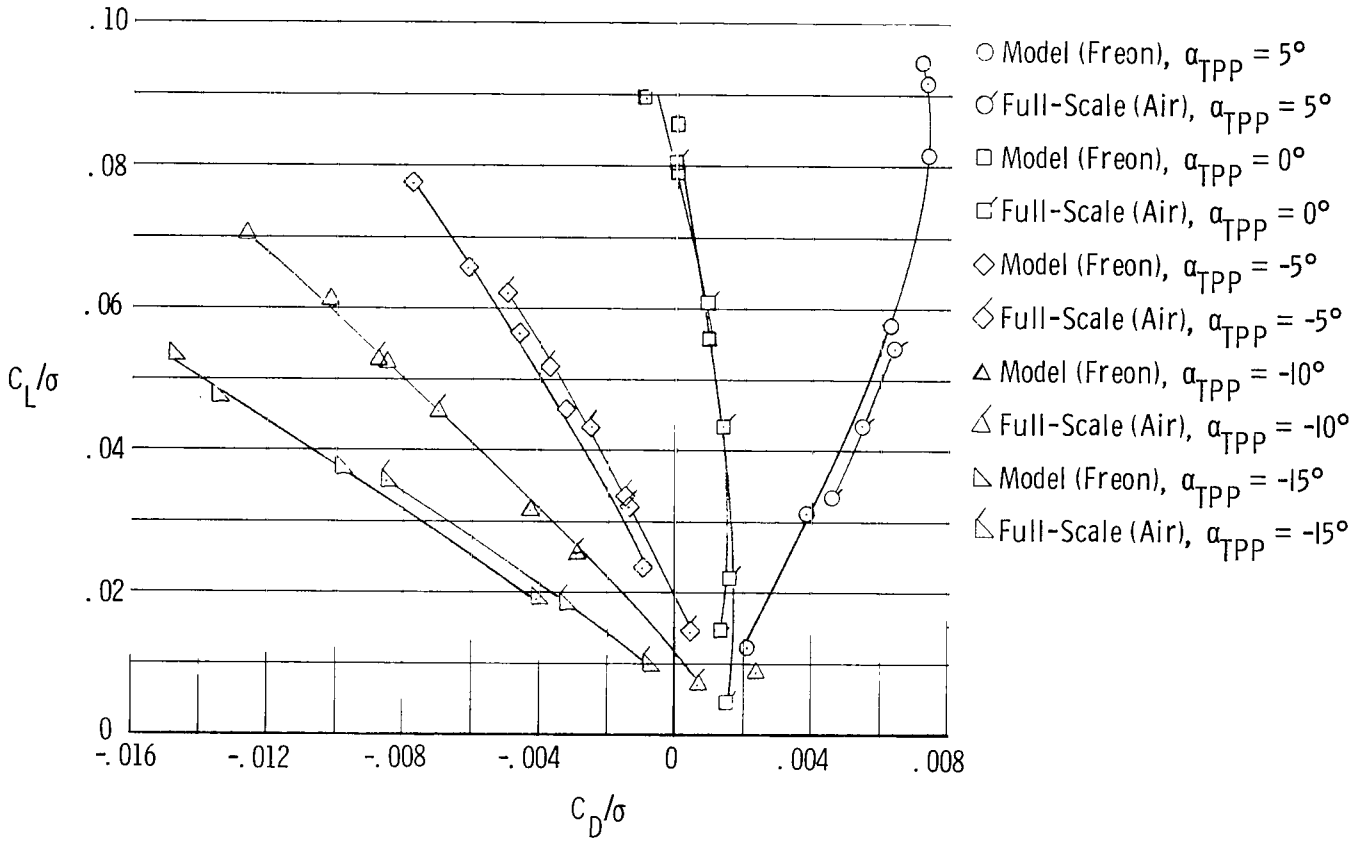

(b) $\mu = 0.30$, $M_{(1.0,\ 90)} = 0.85$.

Figure 5.- Continued.

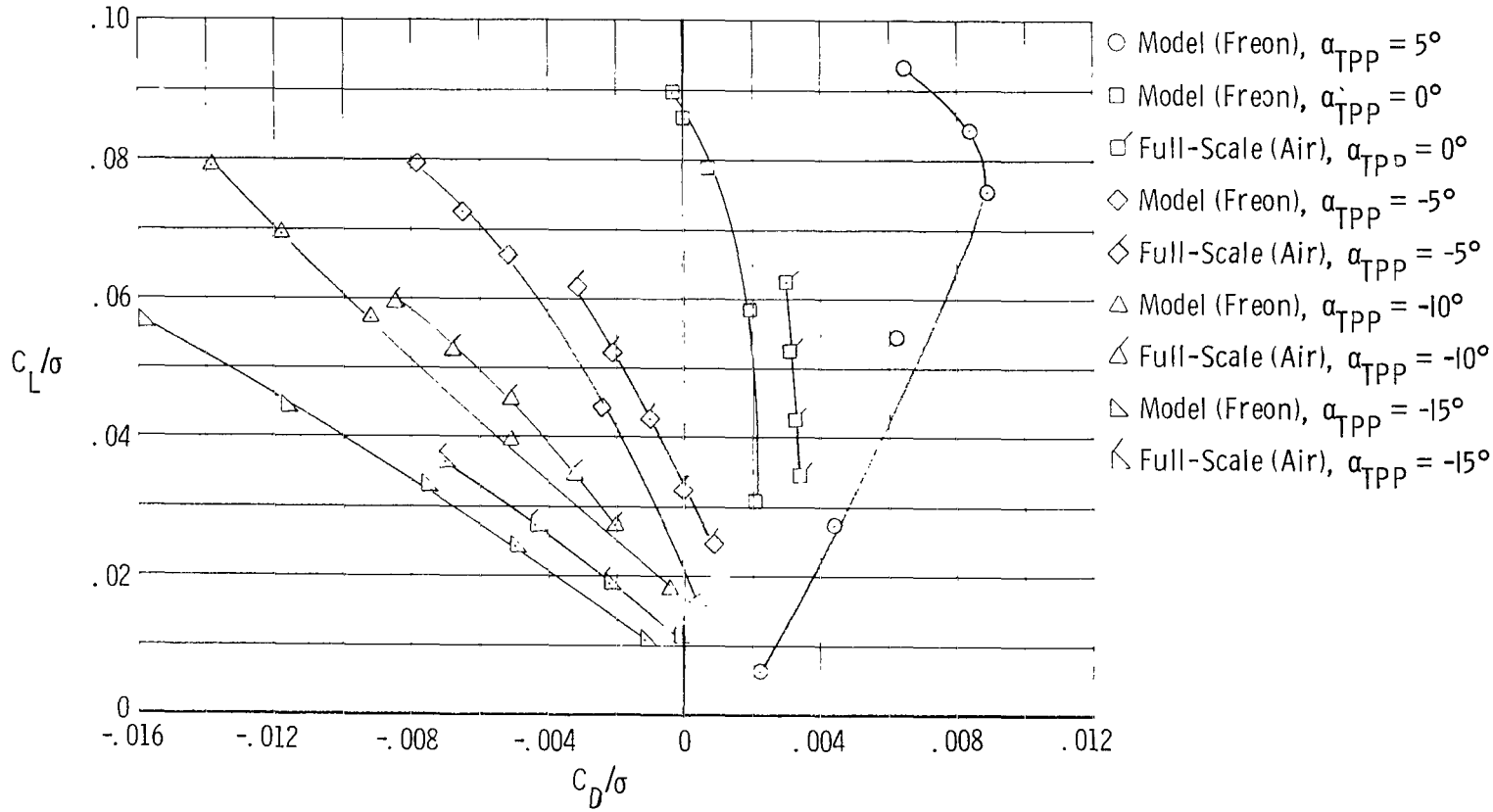

(c) $\mu = 0.30$, $M_{(1.0,\ 90)} = 0.95$.

Figure 5.- Continued.

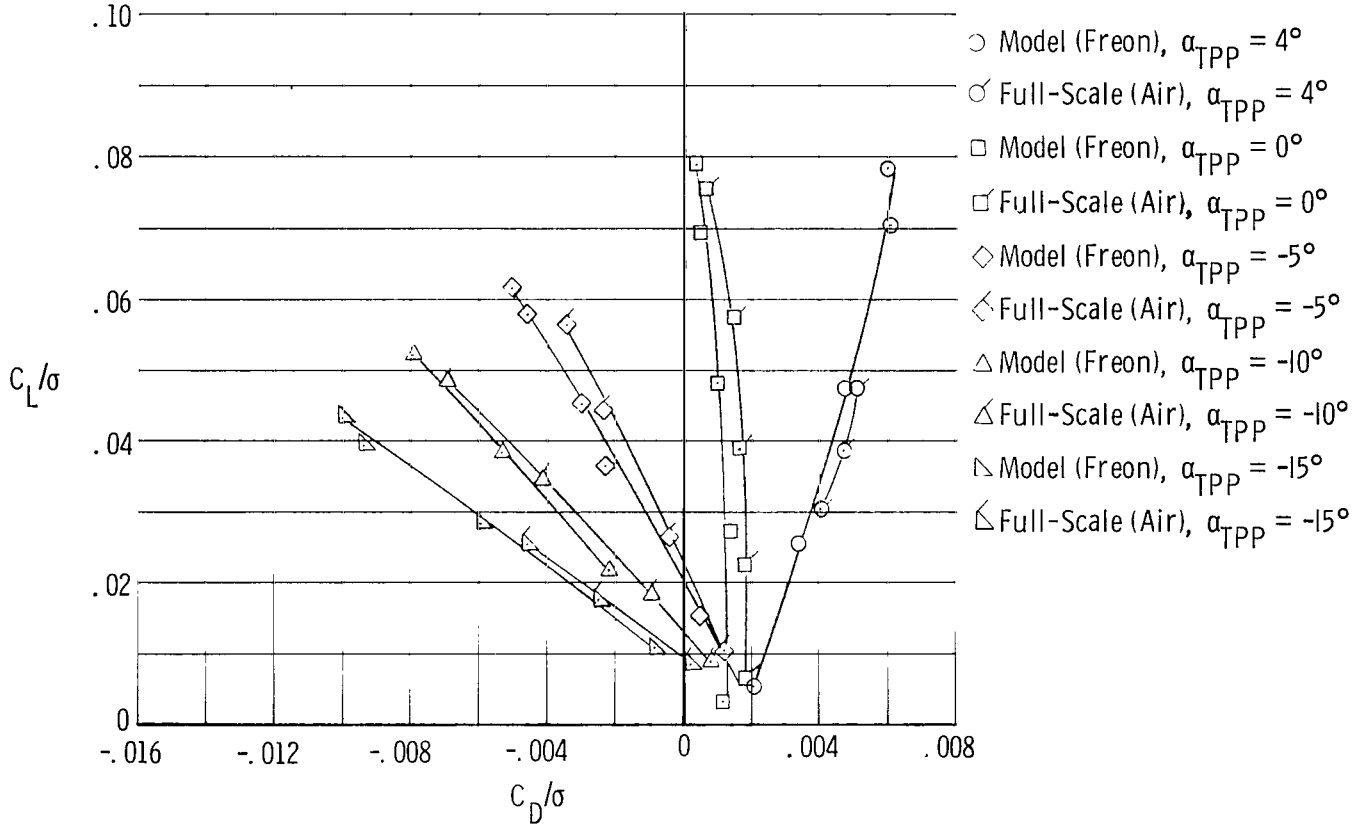

(d) $\mu = 0.35$, $M_{(1.0,\ 90)} = 0.85$.

Figure 5.- Continued.

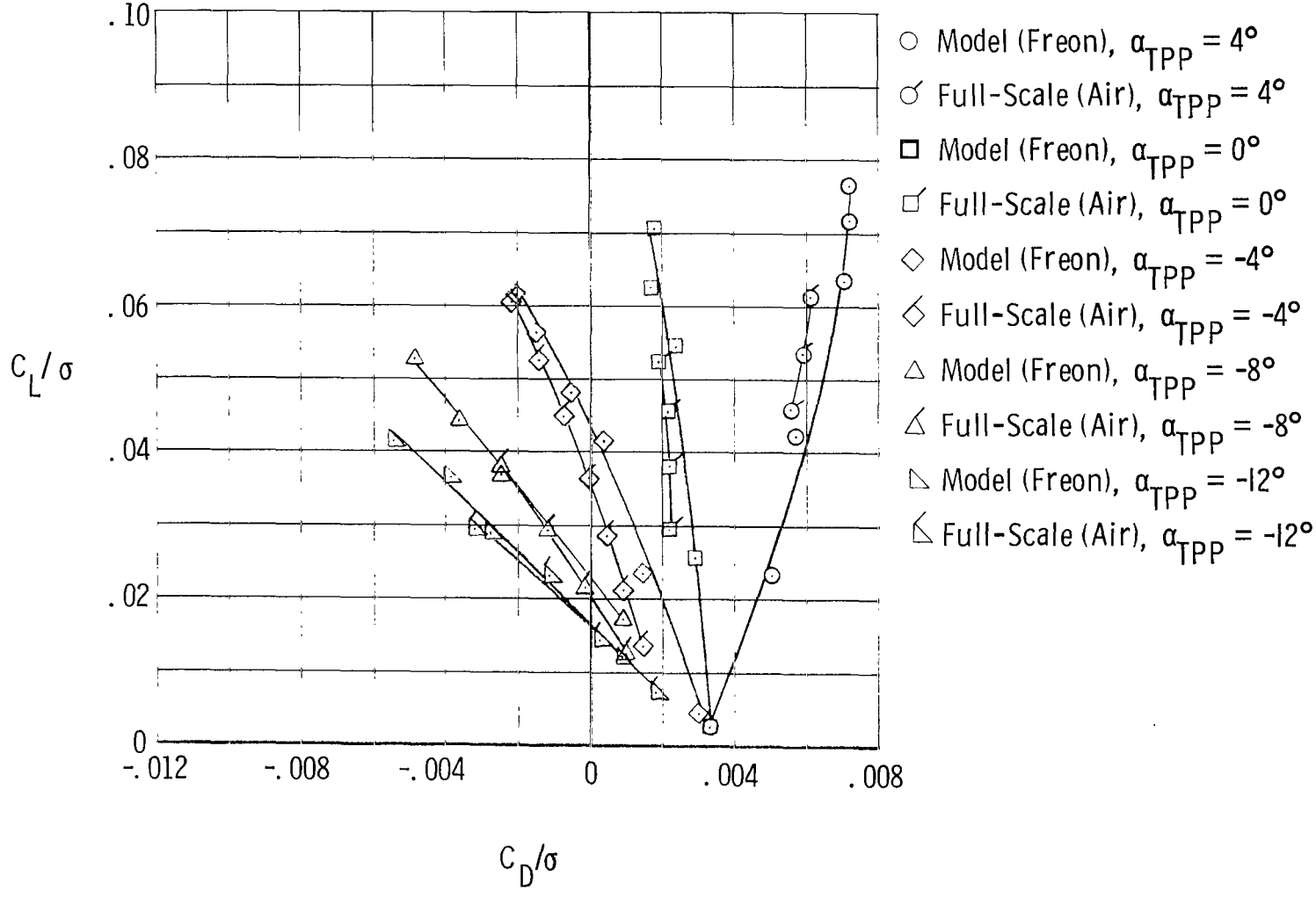

(e) $\mu = 0.40$, $M_{(1.0, 90)} = 0.85$.

Figure 5.- Concluded.

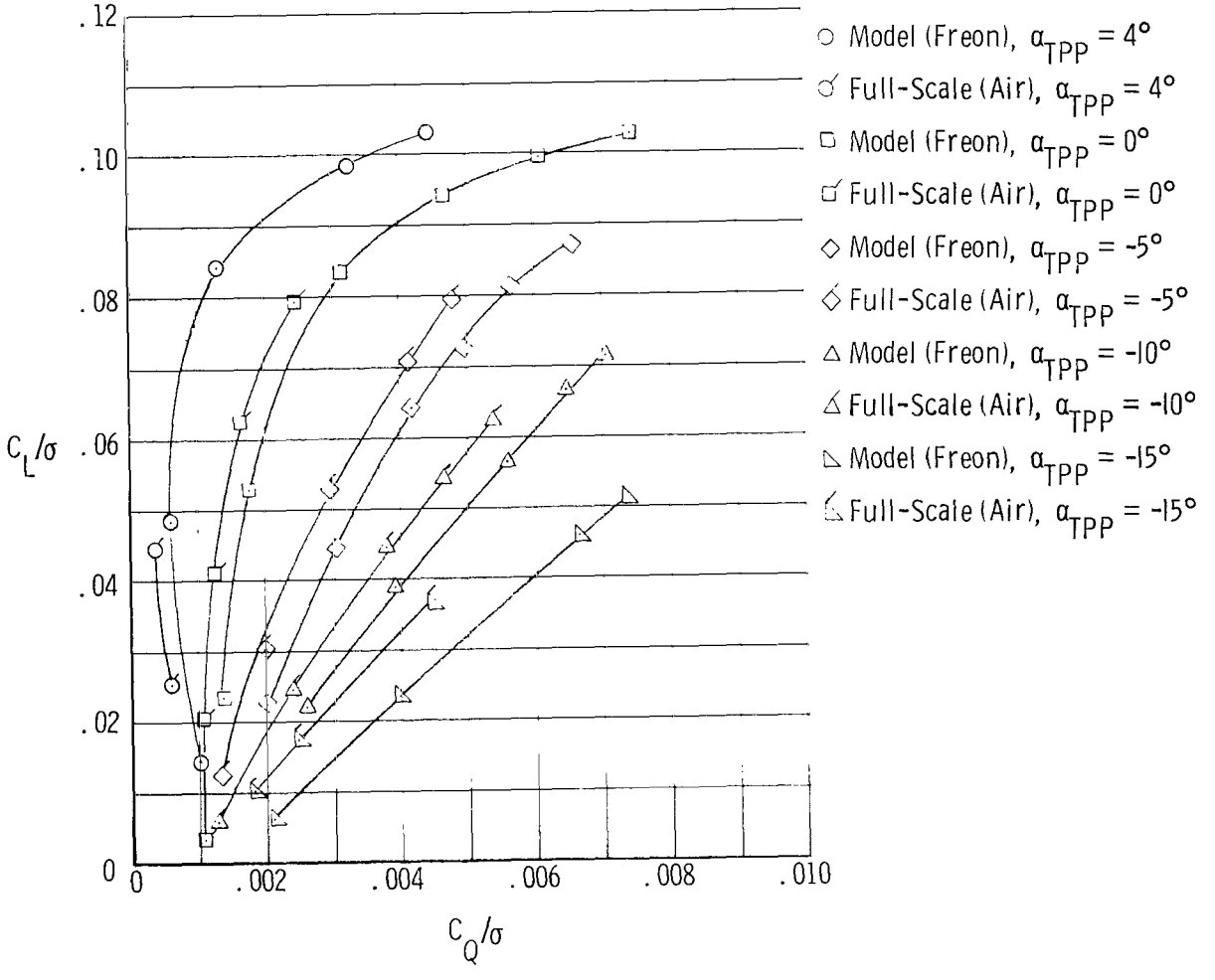

(a) μ = 0.30, $M_{(1.0,\ 90)}$ = 0.79.

Figure 6.- Comparison of freon model and full-scale values of C_L/σ and C_Q/σ for various values of α_{TPP}.

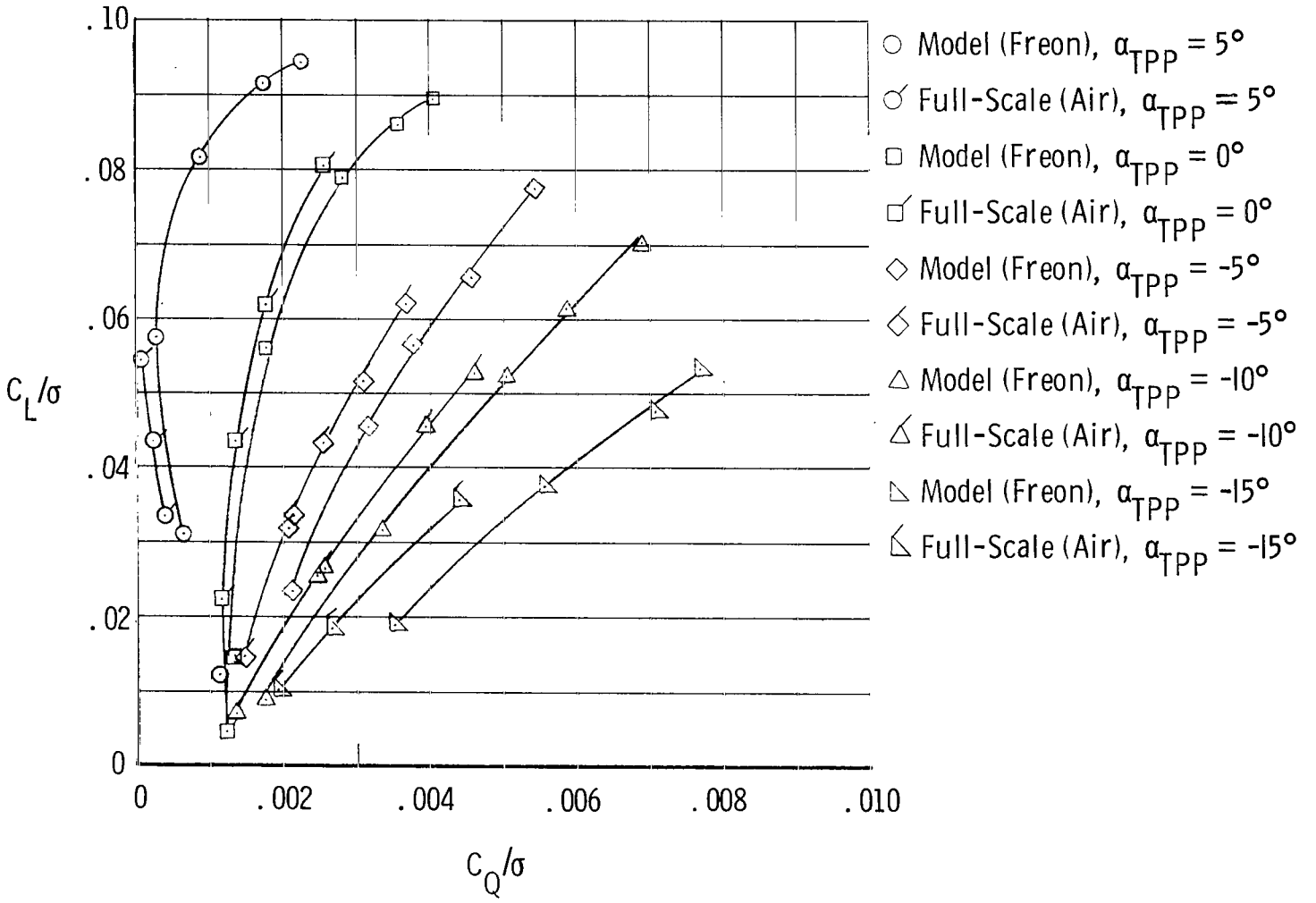

(b) $\mu = 0.30$, $M_{(1.0, 90)} = 0.85$.

Figure 6.- Continued.

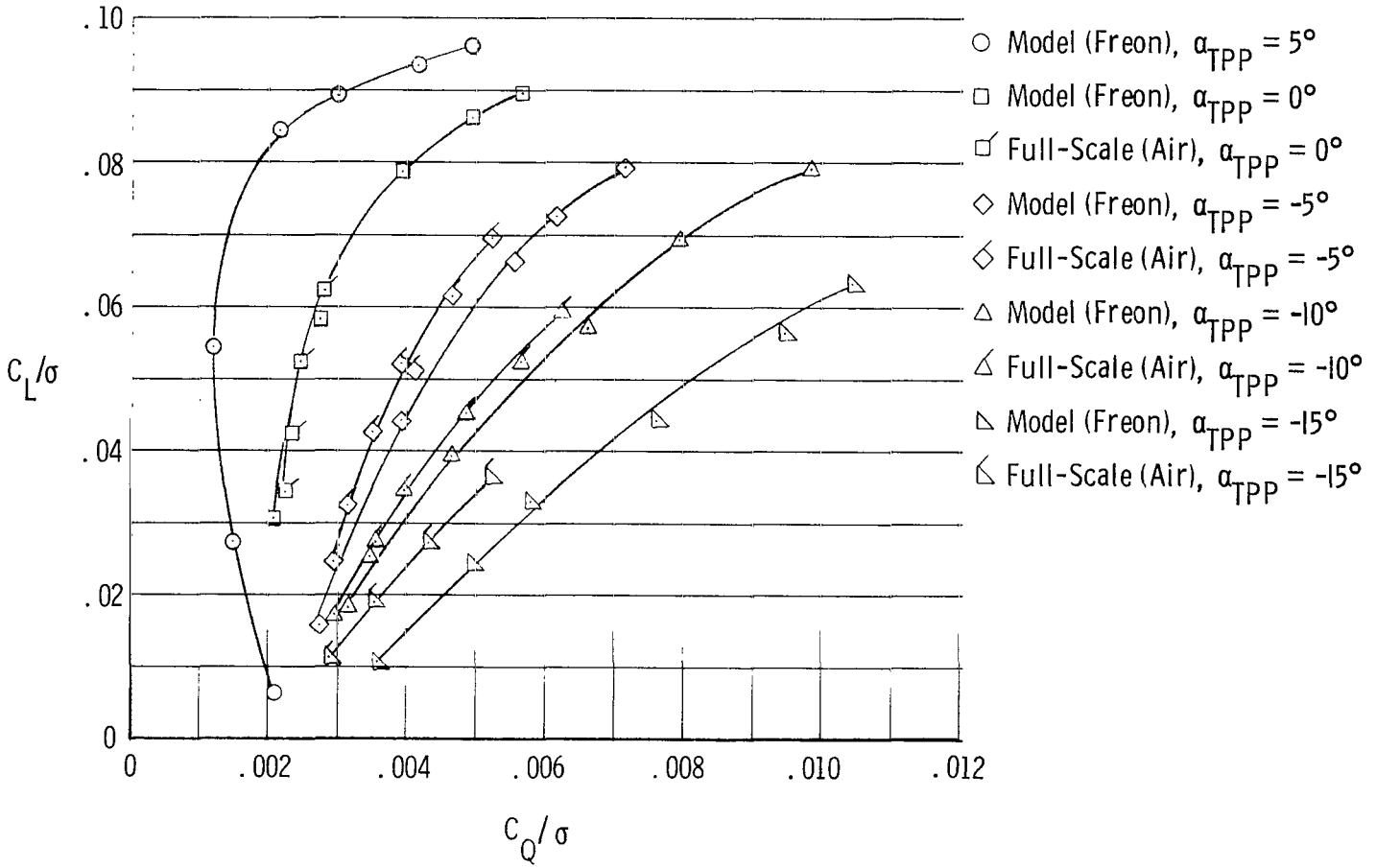

(c) $\mu = 0.30$, $M_{(1.0,\ 90)} = 0.95$.

Figure 6.- Continued.

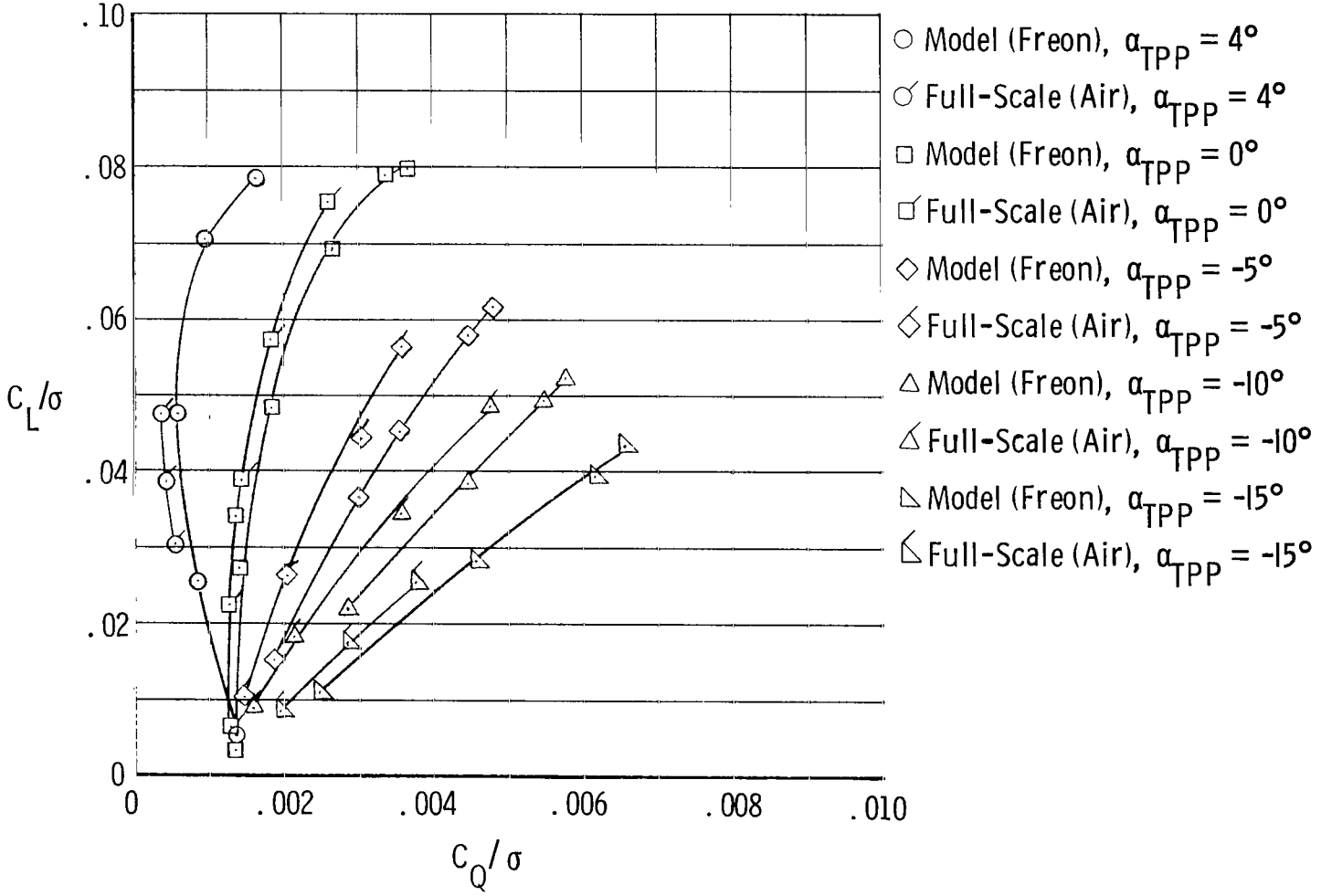

(d) $\mu = 0.35$, $M_{(1.0, 90)} = 0.85$.

Figure 6.- Continued.

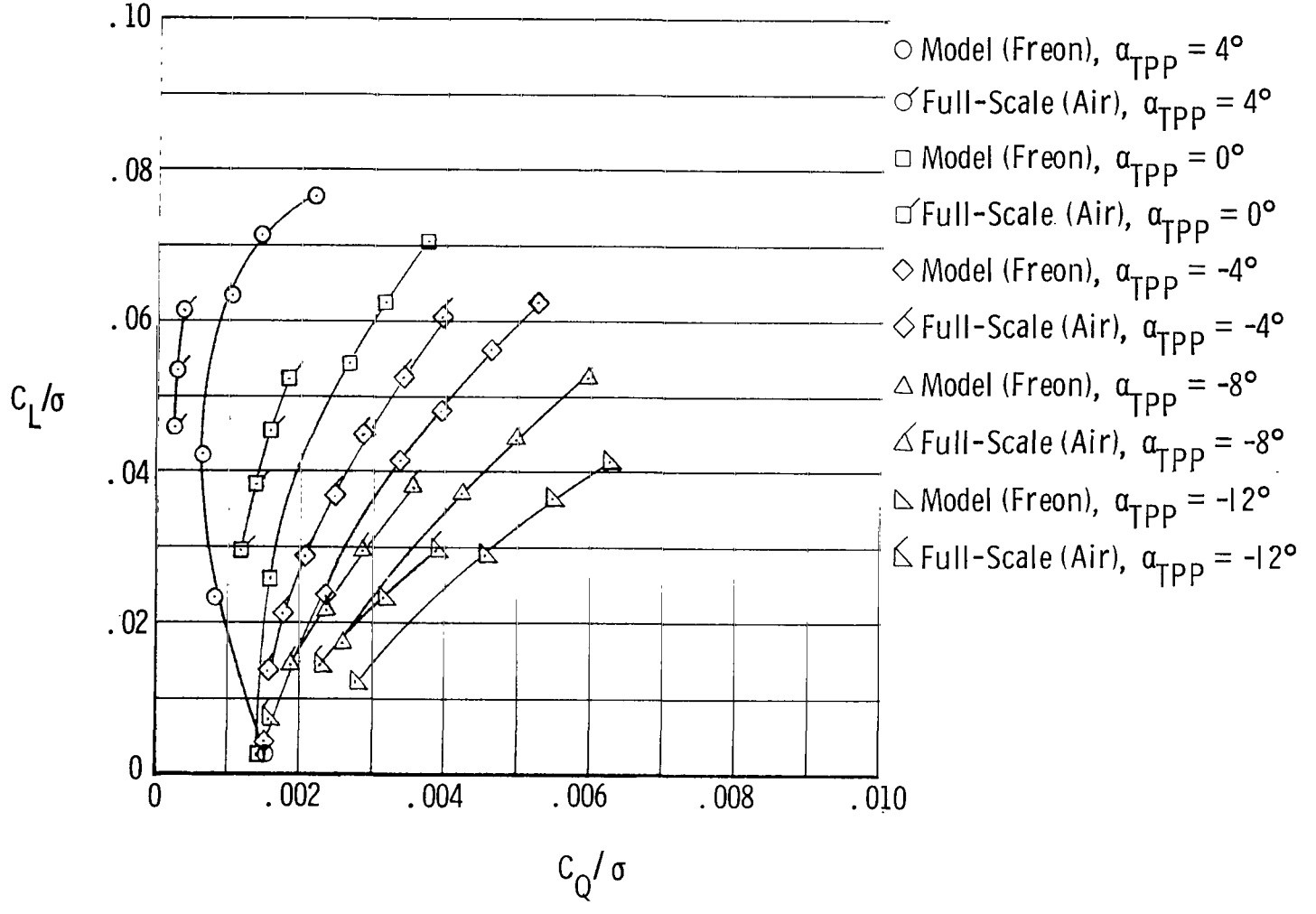

(e) $\mu = 0.40$, $M_{(1.0, 90)} = 0.85$.

Figure 6.- Concluded.

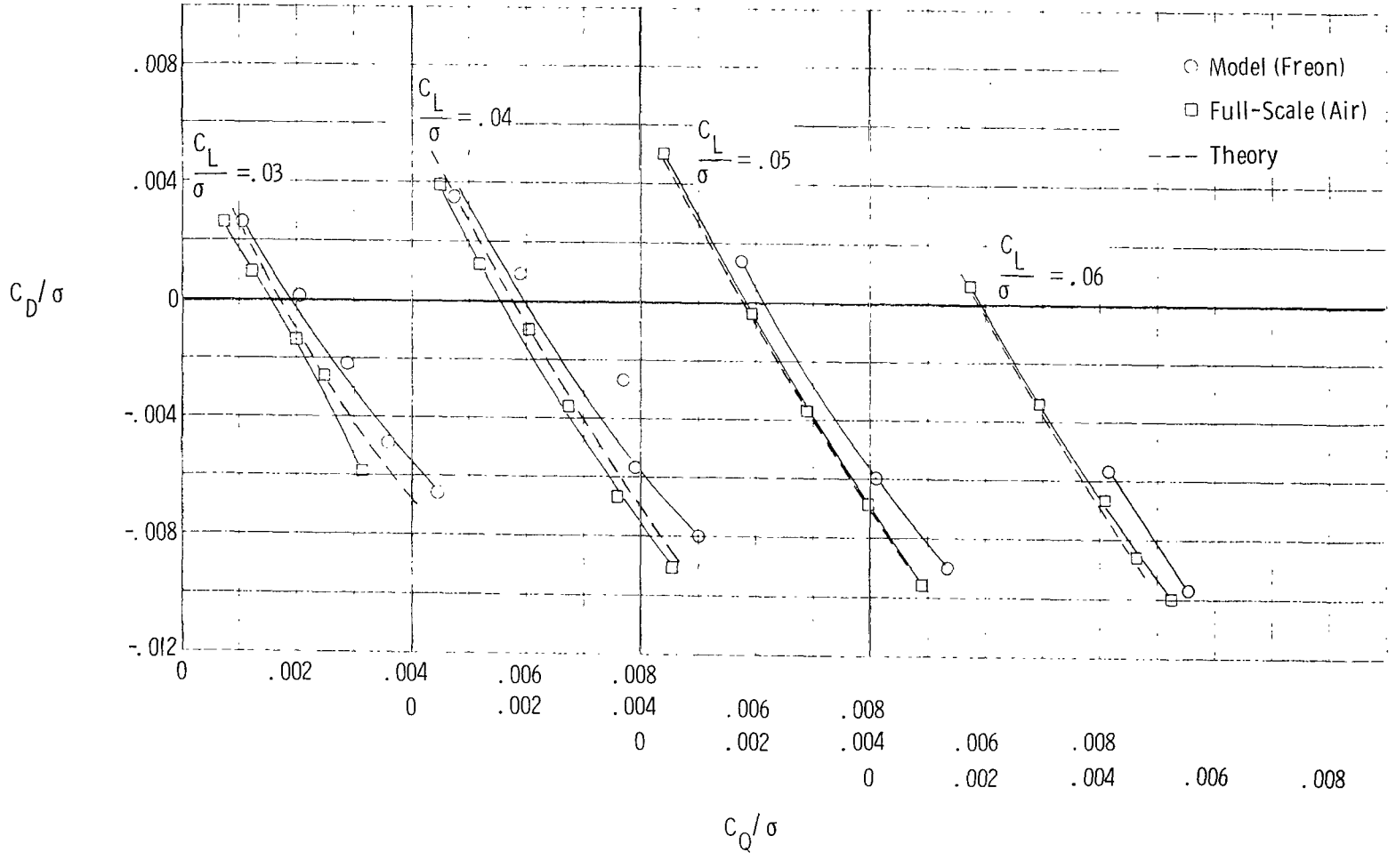

(a) $\mu = 0.30$, $M_{(1.0,\ 90)} = 0.79$.

Figure 7.- Comparison of freon model, full-scale, and theoretical performance for various values of C_L/σ.

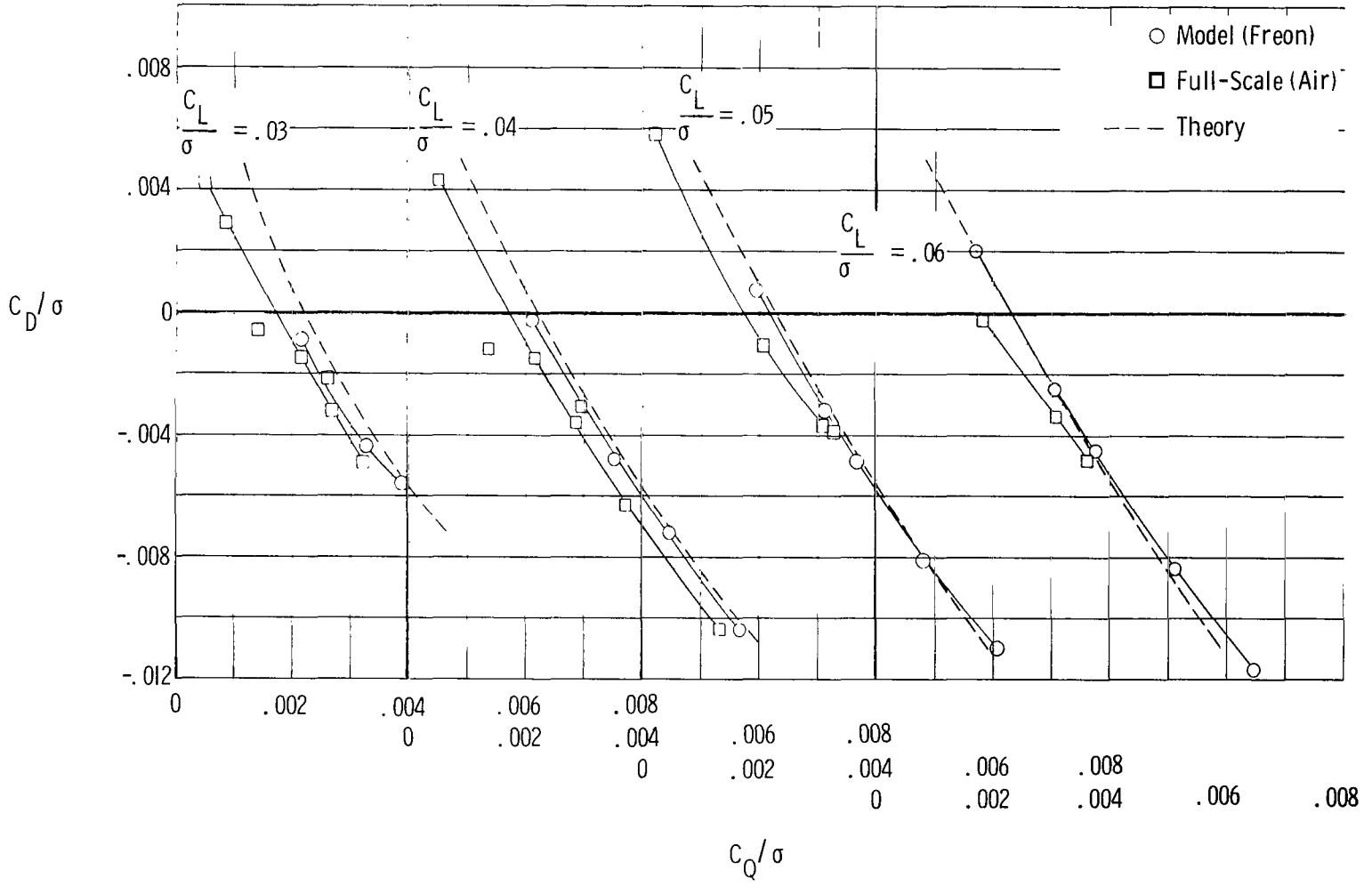

(b) $\mu = 0.30$, $M_{(1.0,\ 90)} = 0.85$.

Figure 7.- Continued.

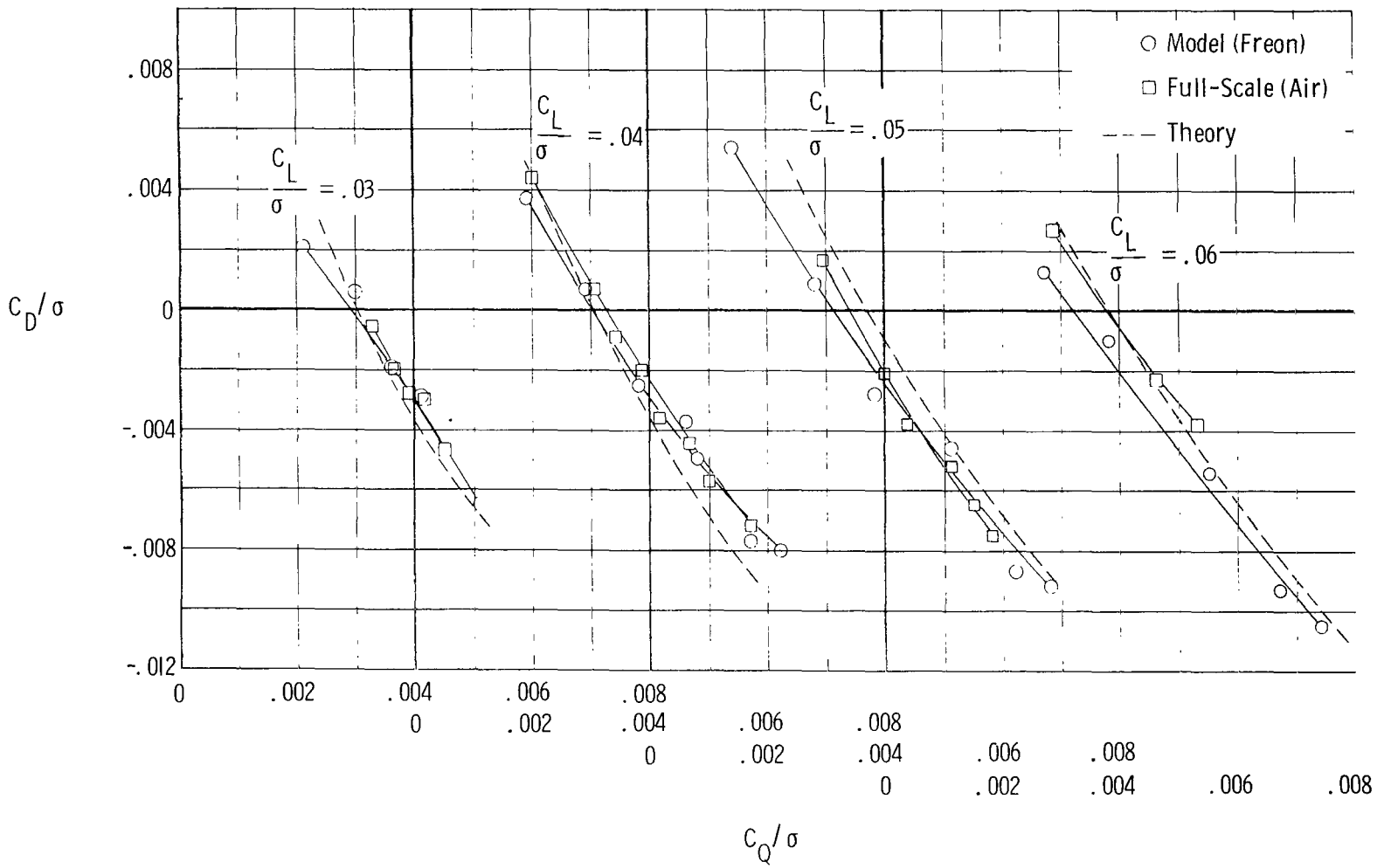

(c) $\mu = 0.30$, $M_{(1.0,\ 90)} = 0.95$.

Figure 7.- Continued.

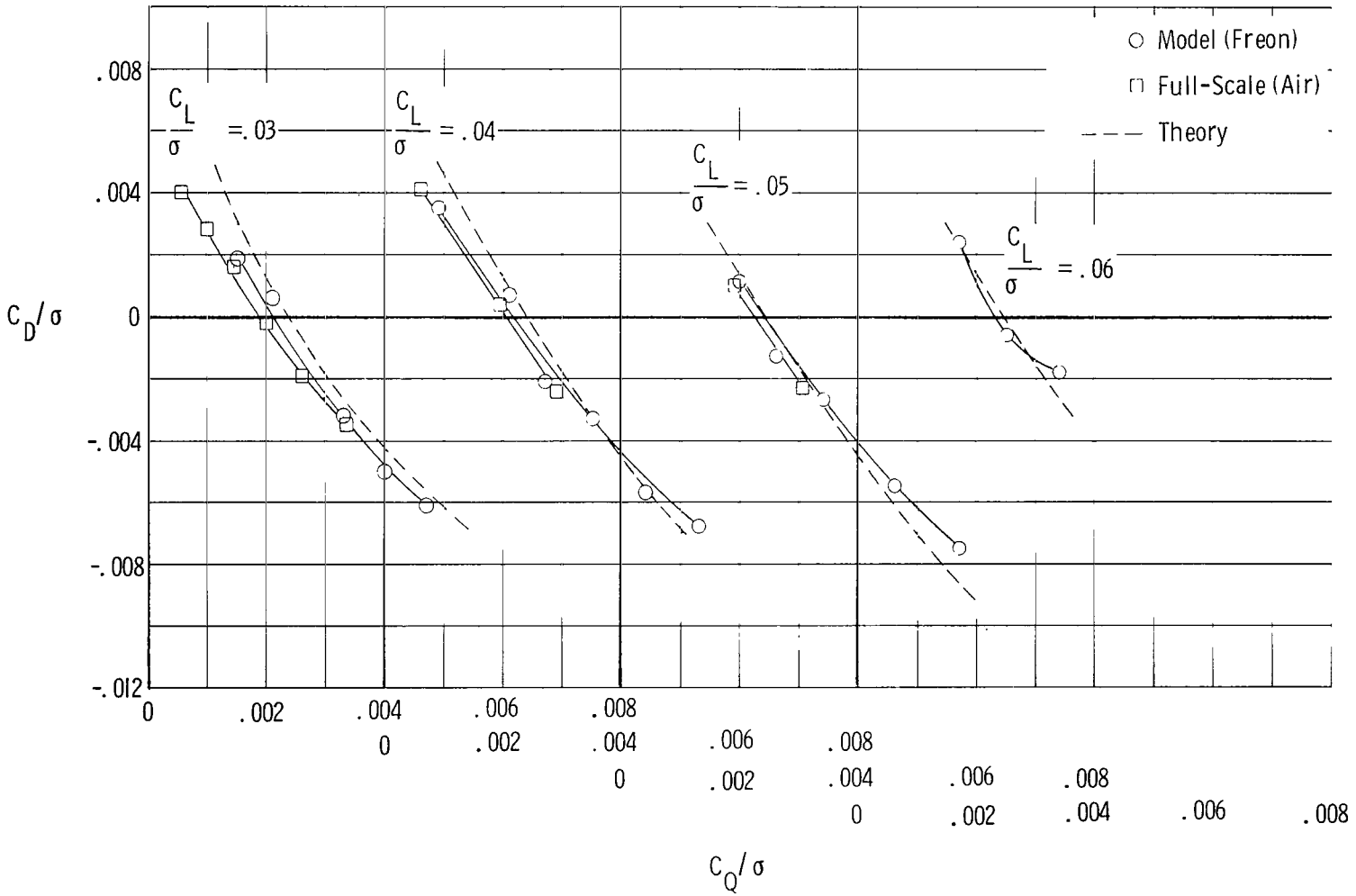

(d) $\mu = 0.35$, $M_{(1.0,\ 90)} = 0.85$.

Figure 7.- Continued.

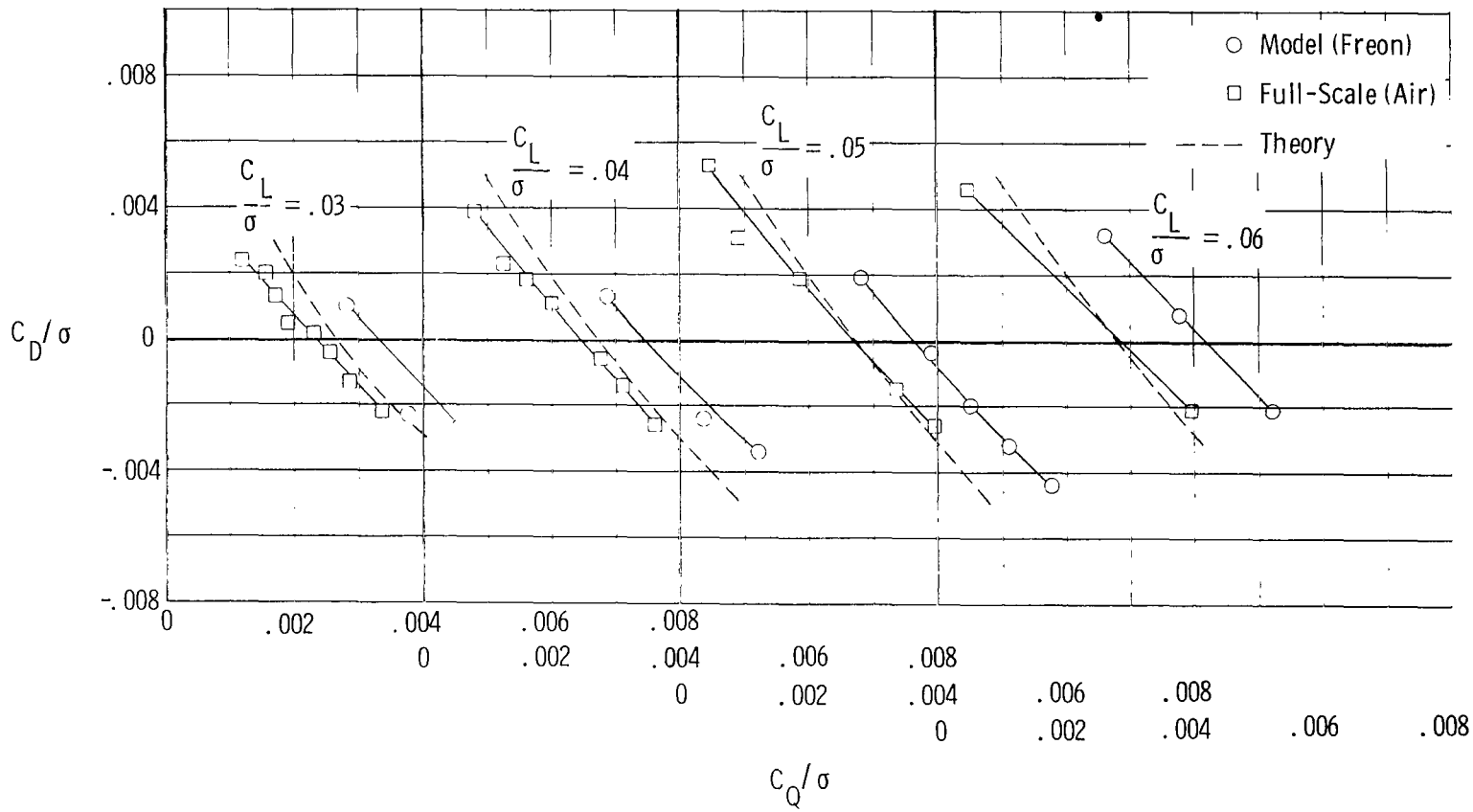

(e) $\mu = 0.40$, $M_{(1.0, 90)} = 0.85$.

Figure 7.- Concluded.

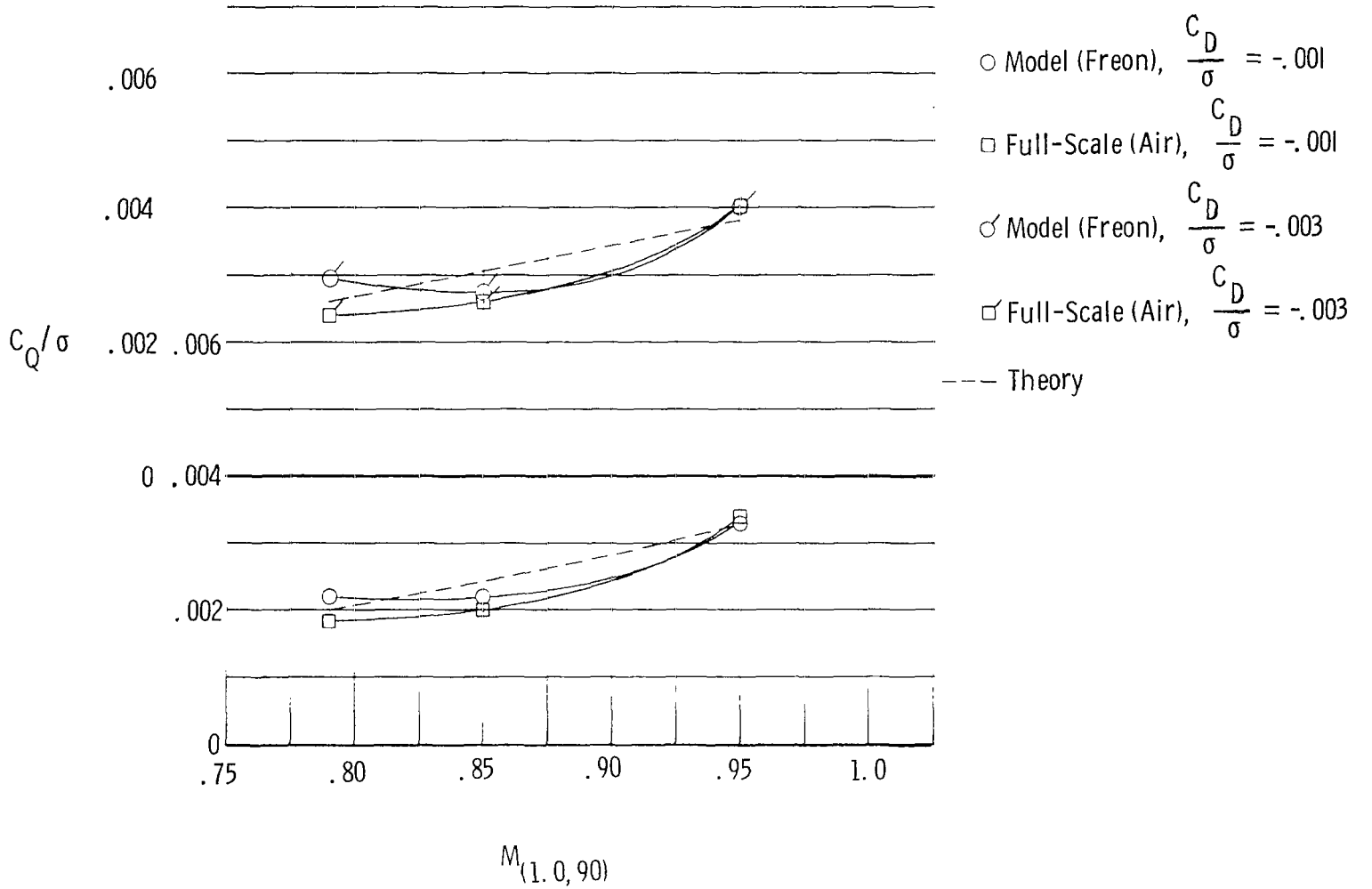

(a) $C_L/\sigma = 0.03$, $\mu = 0.30$.

Figure 8.- Effect of $M_{(1.0, 90)}$ on freon model, full-scale, and theoretical performance for various values of C_L/σ and C_D/σ.

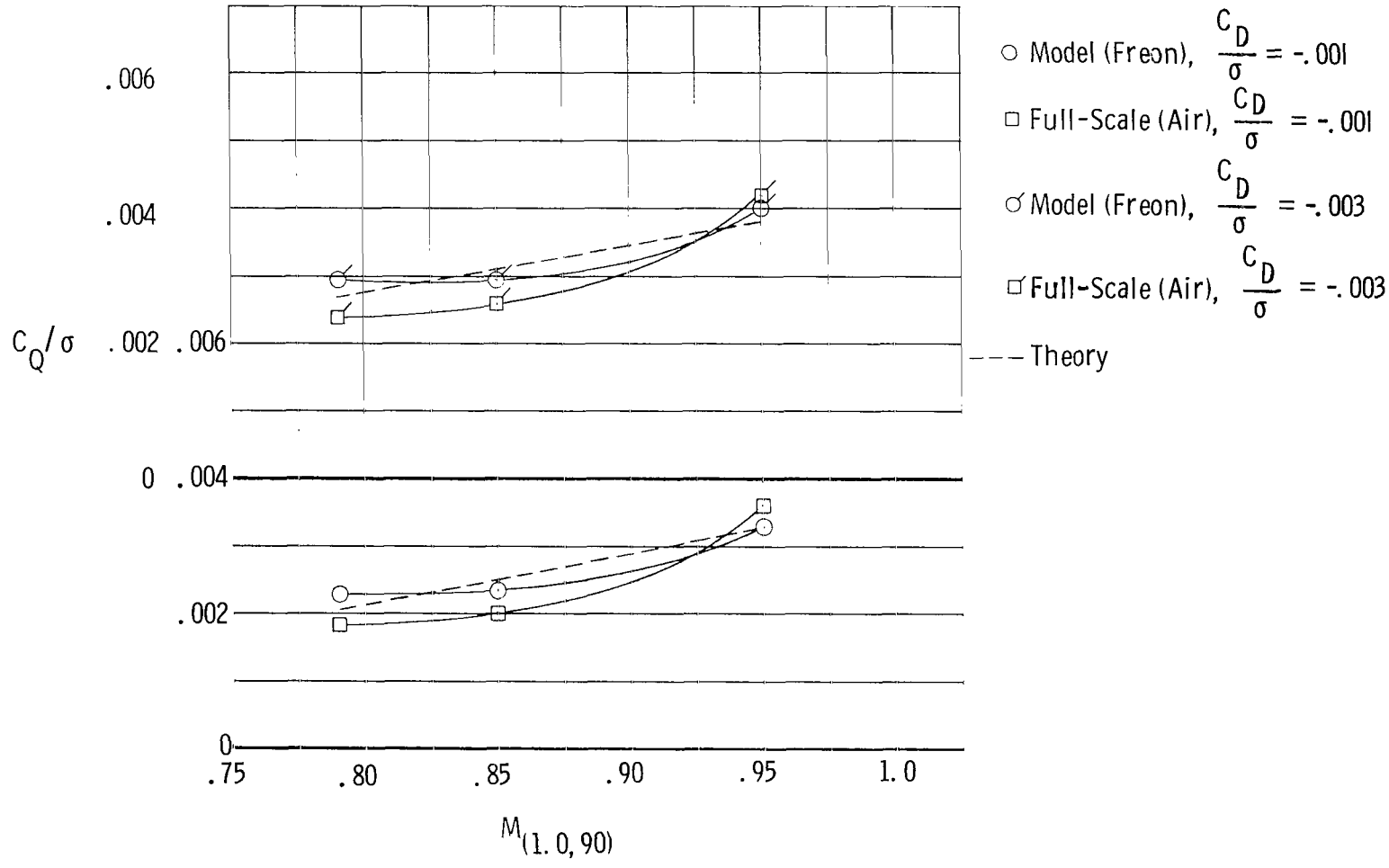

(b) $C_L/\sigma = 0.04$, $\mu = 0.30$.

Figure 8.- Continued.

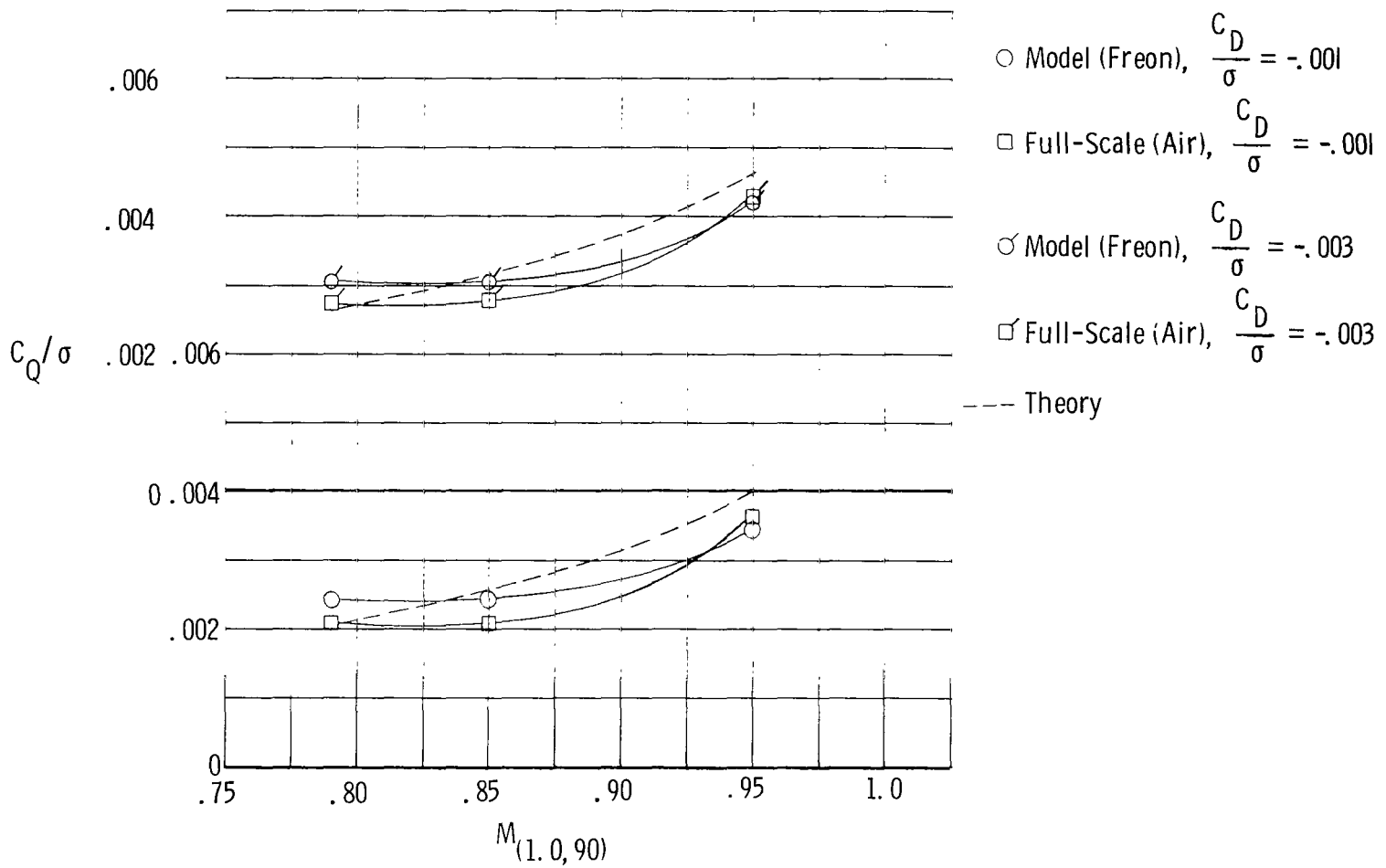

(c) $C_L/\sigma = 0.05$, $\mu = 0.30$.

Figure 8.- Concluded.

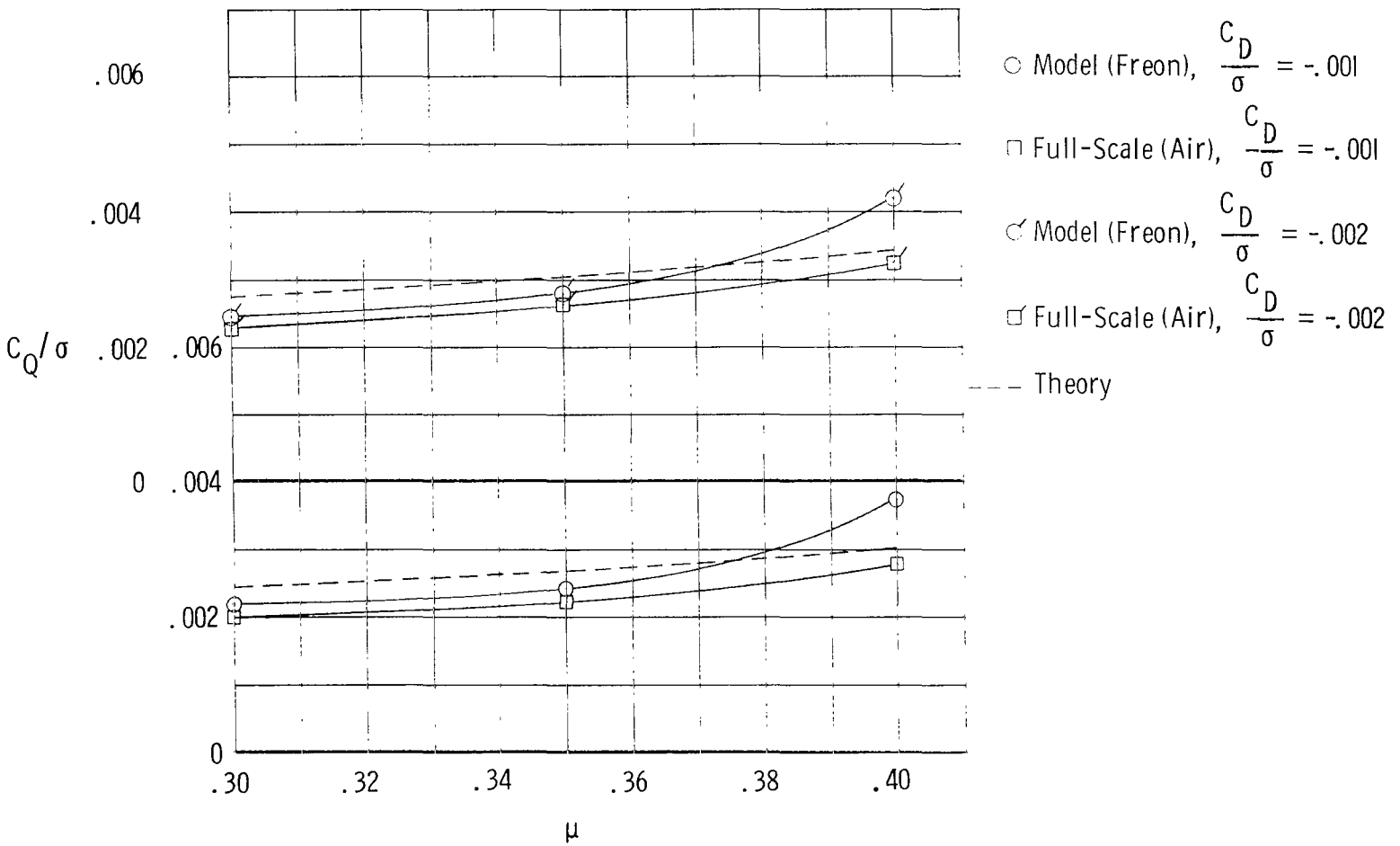

(a) $C_L/\sigma = 0.03$, $M_{(1.0,\ 90)} = 0.85$.

Figure 9.- Effect of μ on freon model, full-scale, and theoretical performance for various values of C_L/σ and C_D/σ.

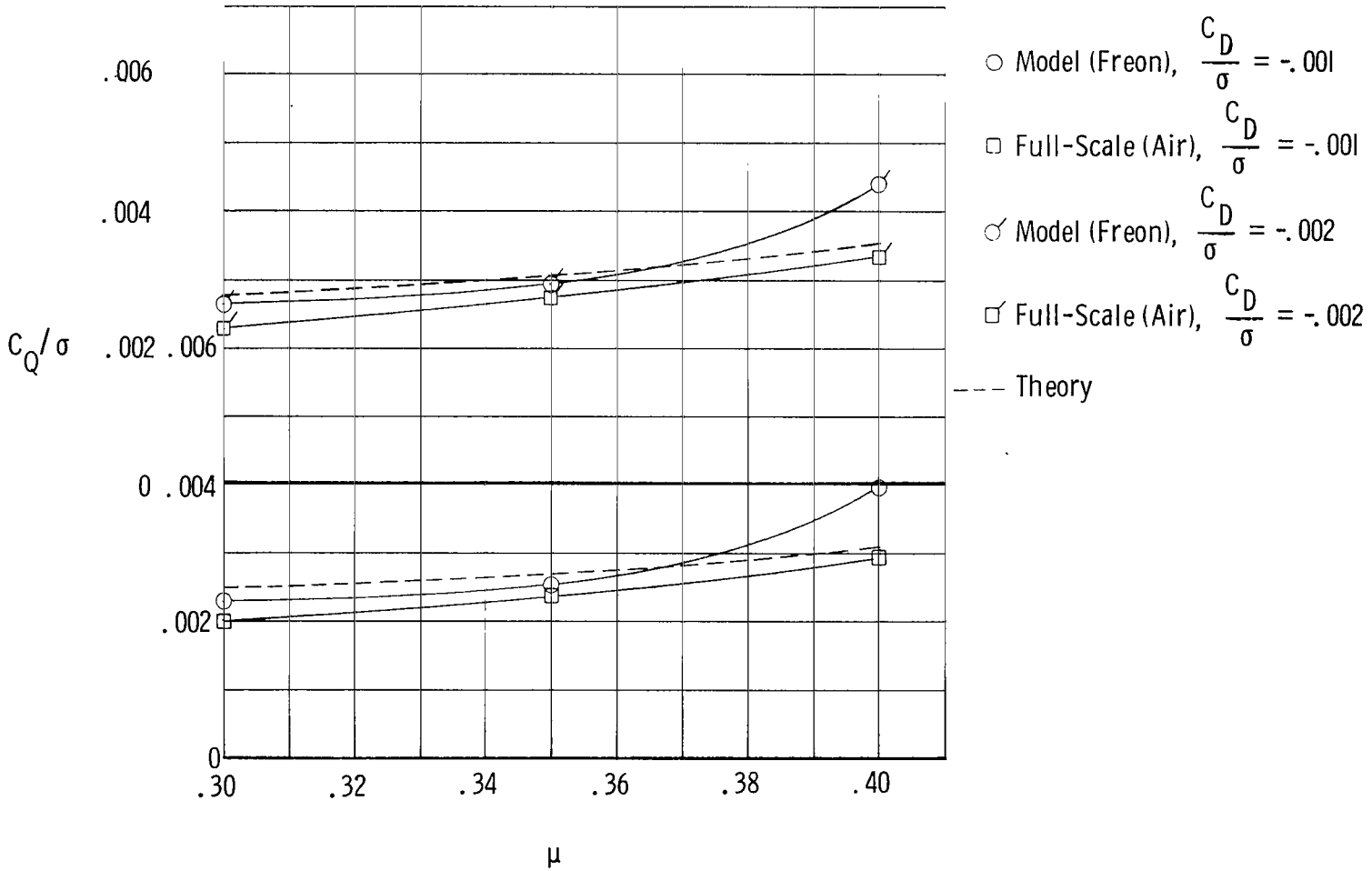

(b) $C_L/\sigma = 0.04$, $M_{(1.0, 90)} = 0.85$.

Figure 9.- Continued.

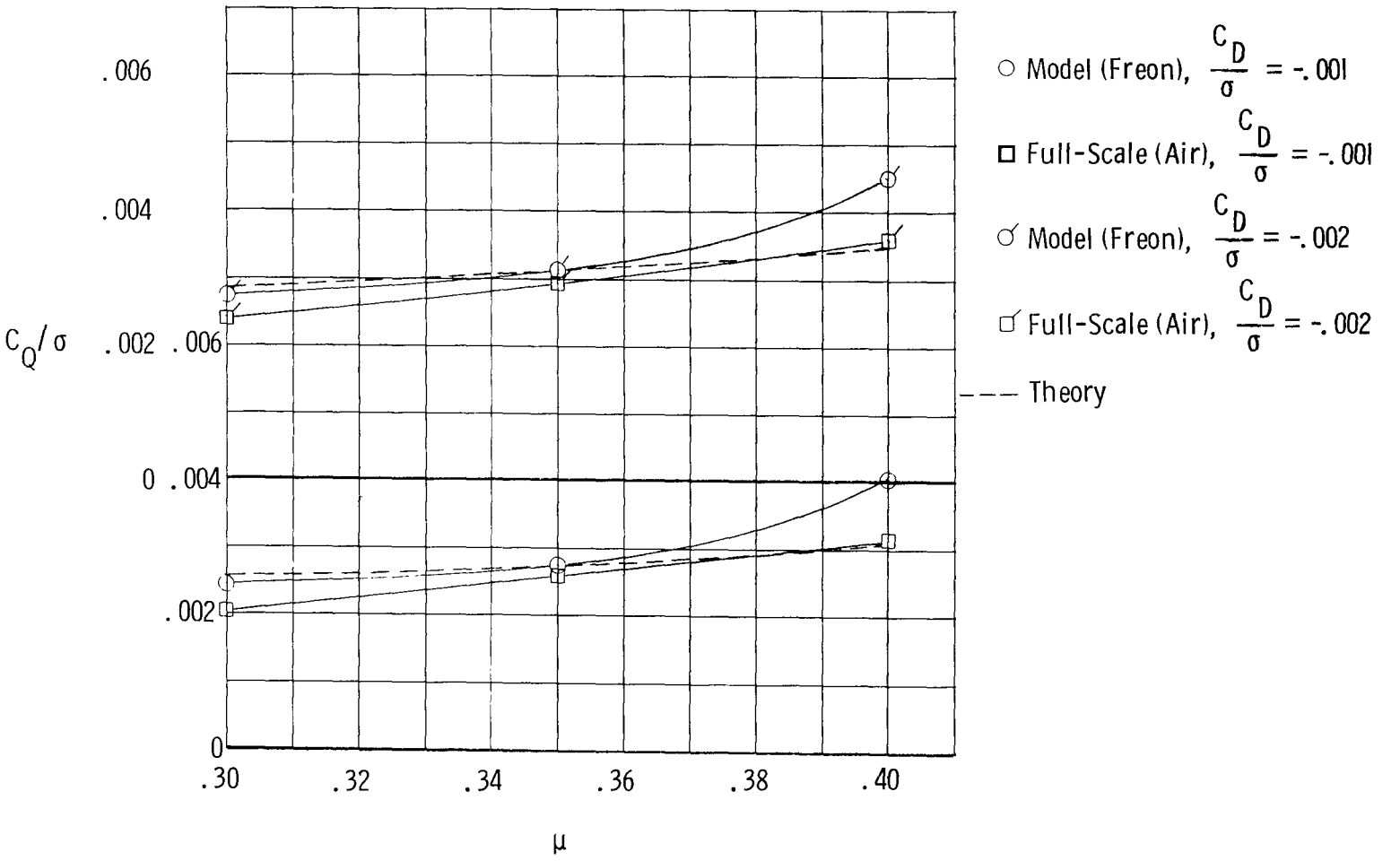

(c) $C_L/\sigma = 0.05$, $M_{(1.0,\ 90)} = 0.85$.

Figure 9.- Concluded.

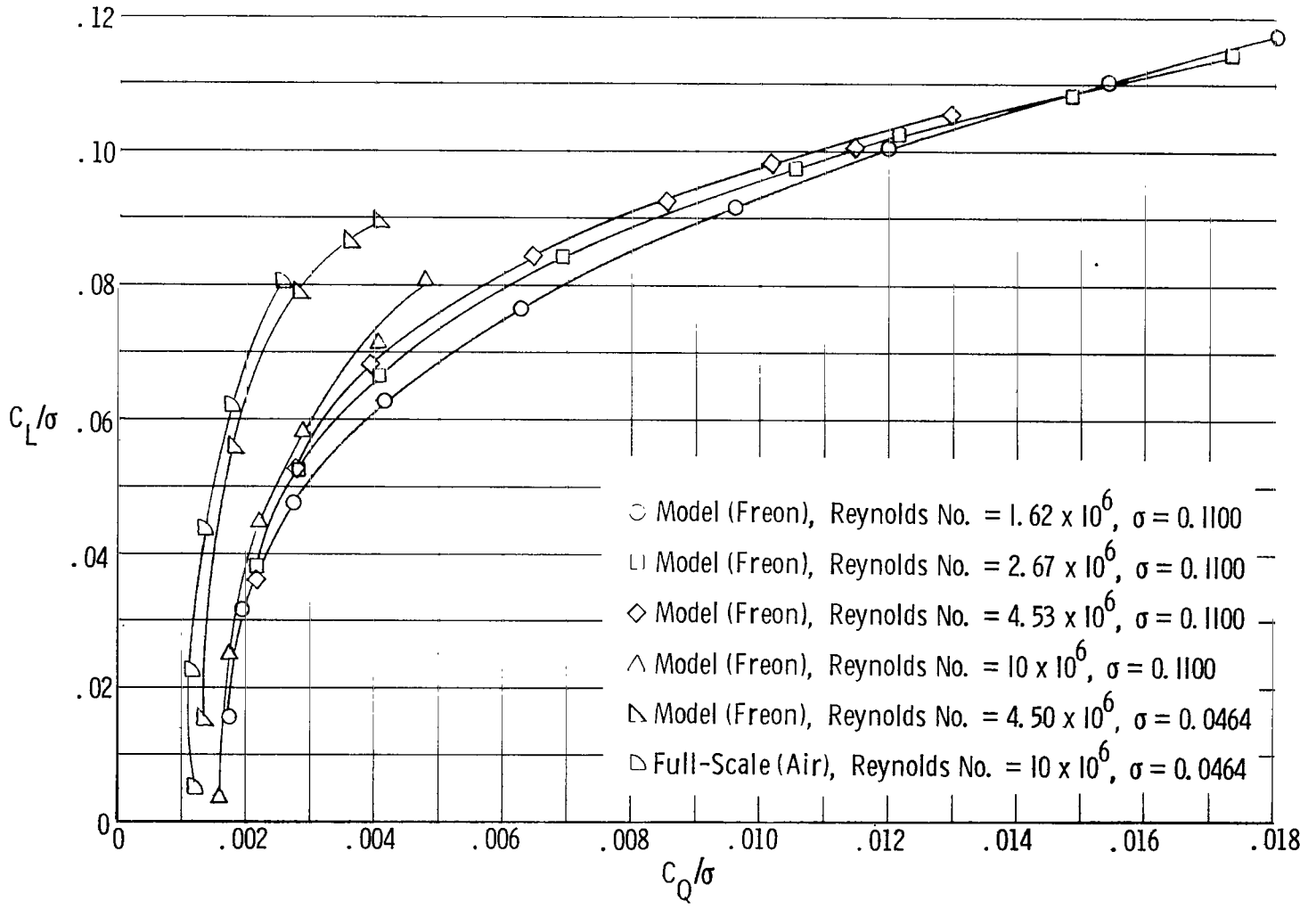

Figure 10.- Effect of scaling parameters on freon model and full-scale rotor performance.
$\left(\mu = 0.30, \quad M_{(1.0,\ 90)} = 0.85, \quad \alpha_{TPP} = 0^{o}.\right)$

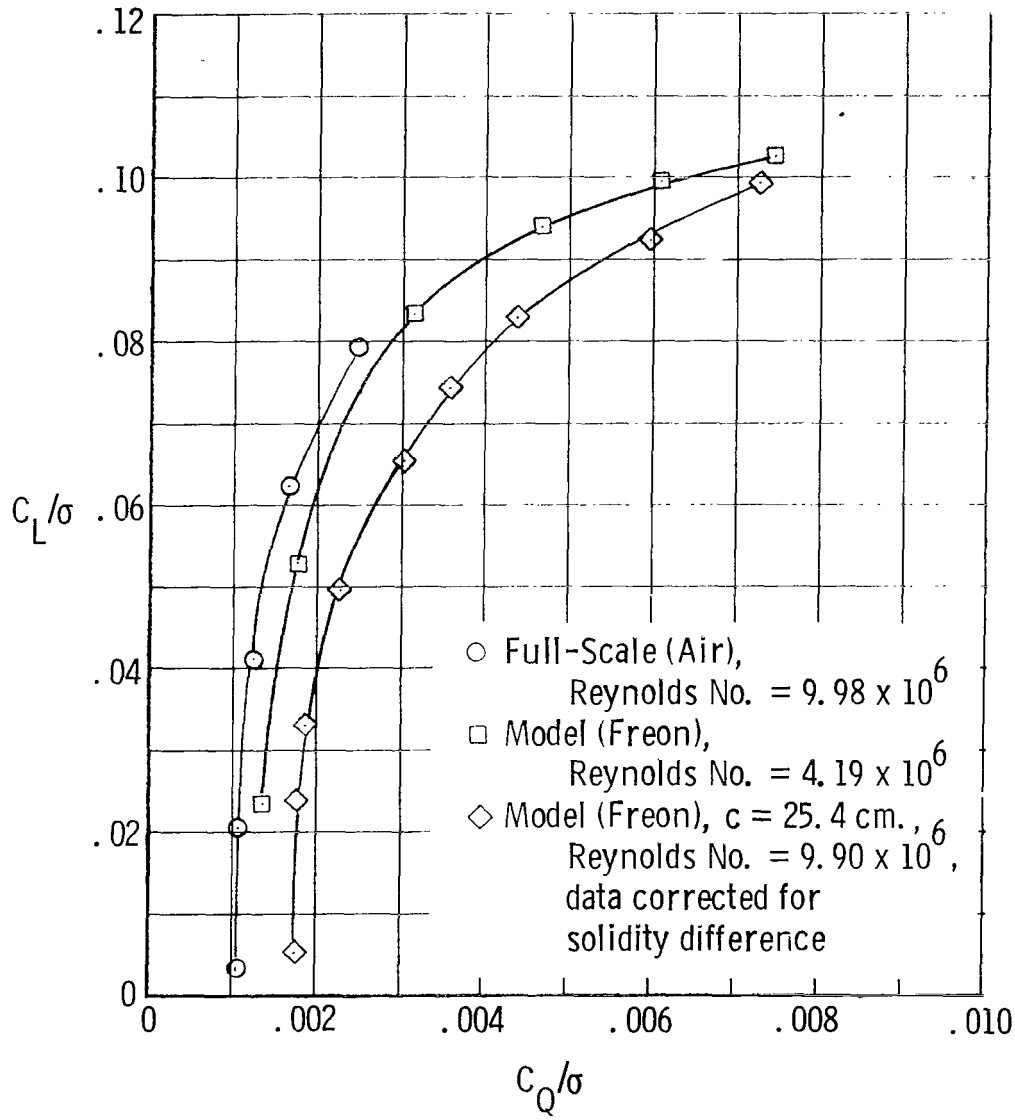

(a) $\mu = 0.30$, $M_{(1.0,\ 90)} = 0.79$, $\alpha_{TPP} = 0^{\circ}$.

Figure 11.- Effect of scaling parameters on freon model and full-scale values of C_L/σ and C_Q/σ.

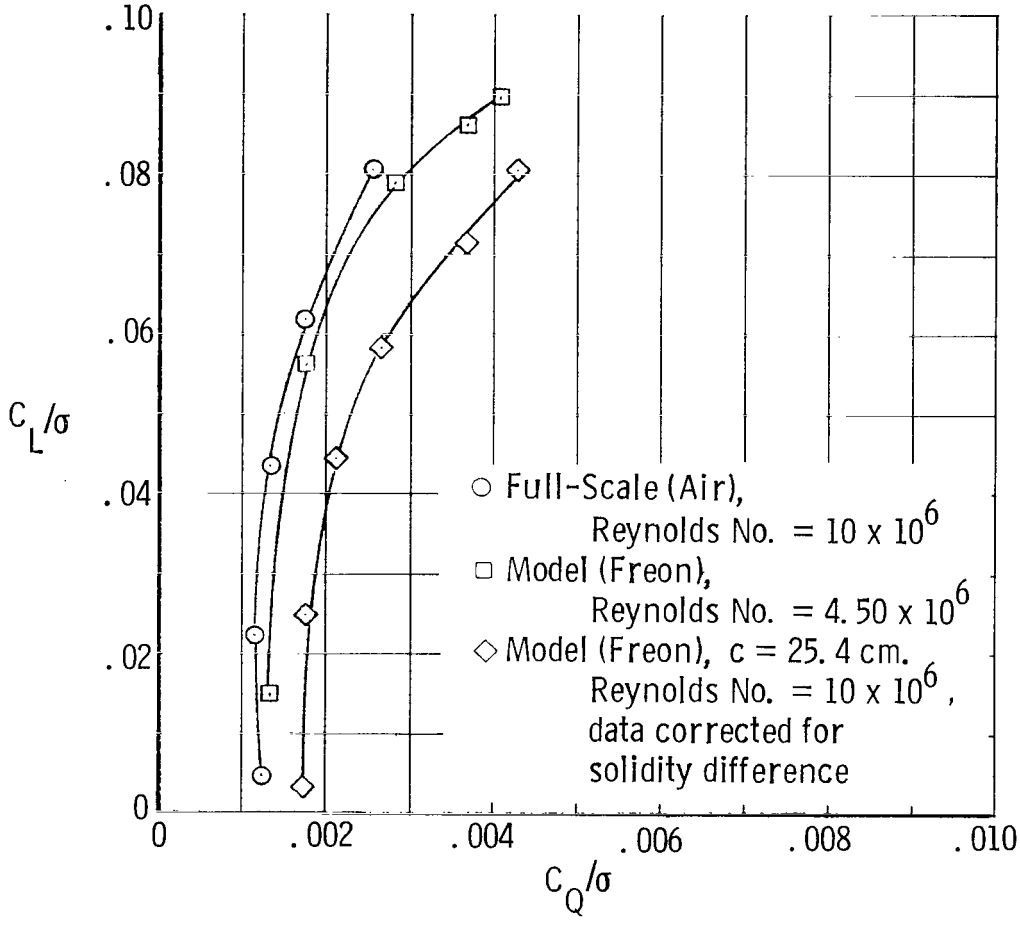

(b) $\mu = 0.30$, $M_{(1.0, 90)} = 0.85$, $\alpha_{TPP} = 0^{\circ}$.

Figure 11.- Continued.

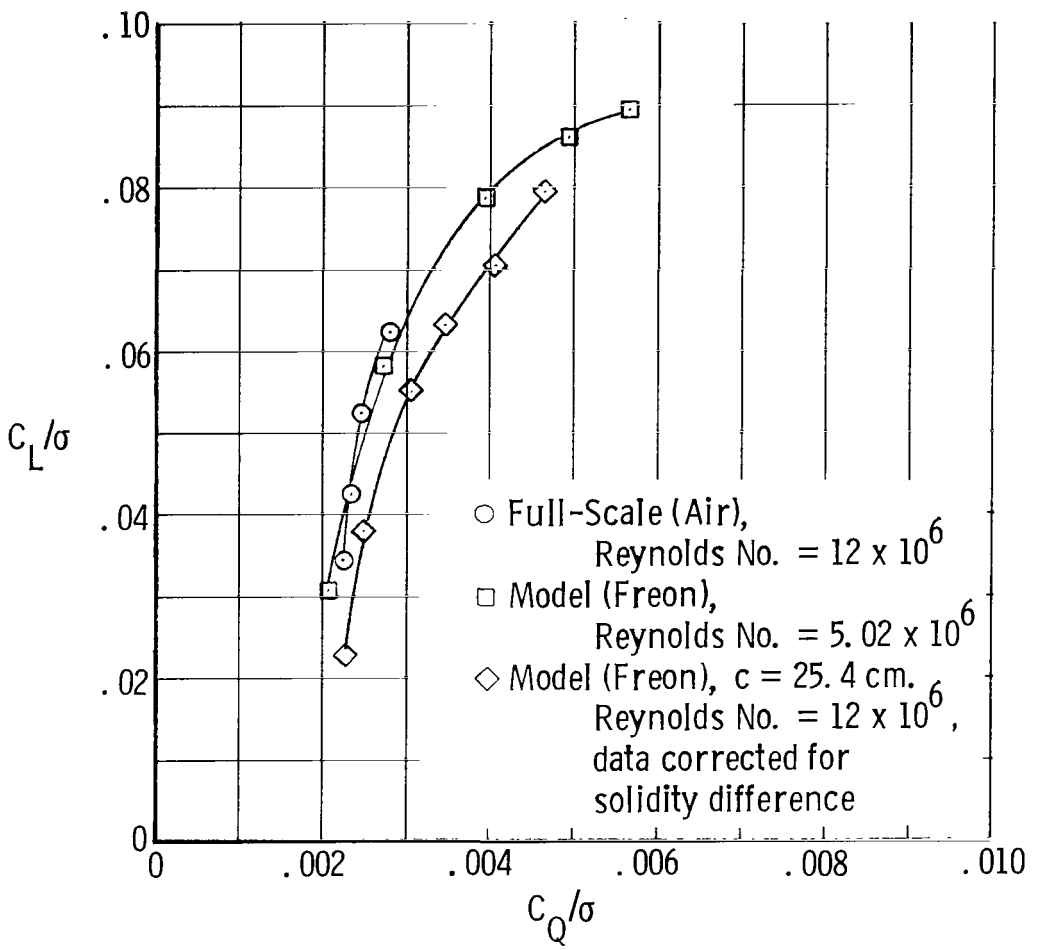

(c) $\mu = 0.30$, $M_{(1.0,\ 90)} = 0.95$, $\alpha_{TPP} = 0^o$.

Figure 11.- Continued.

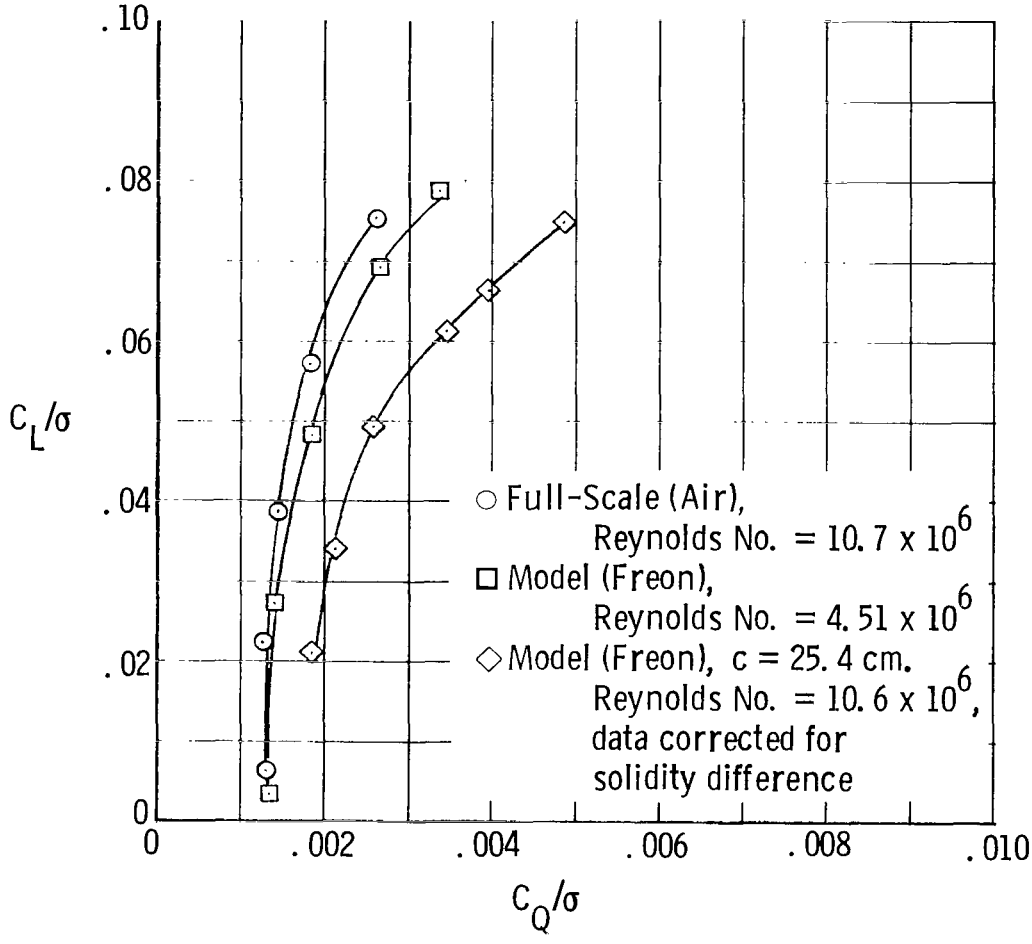

(d) $\mu = 0.35$, $M_{(1.0,\ 90)} = 0.85$, $\alpha_{TPP} = 0^{\circ}$.

Figure 11.- Continued.

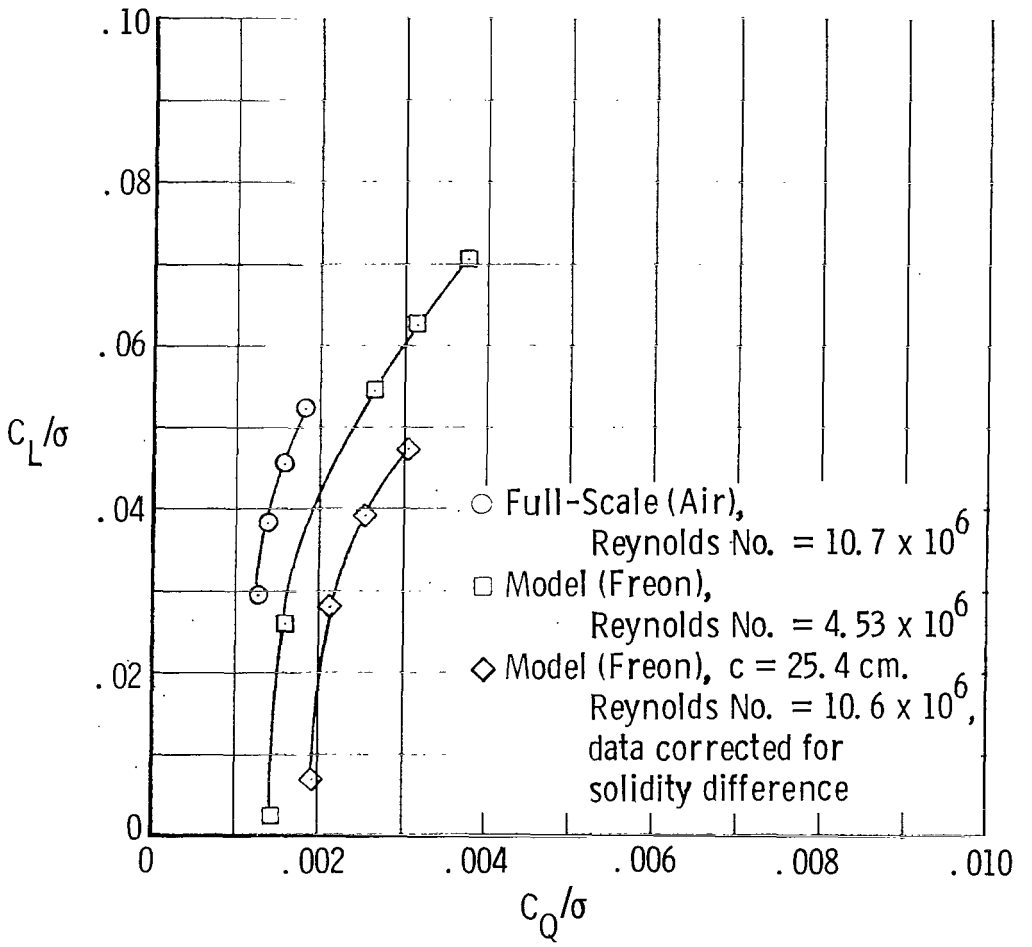

(e) $\mu = 0.40$, $M_{(1.0,\ 90)} = 0.85$, $\alpha_{TPP} = 0^{o}$.

Figure 11.- Concluded.

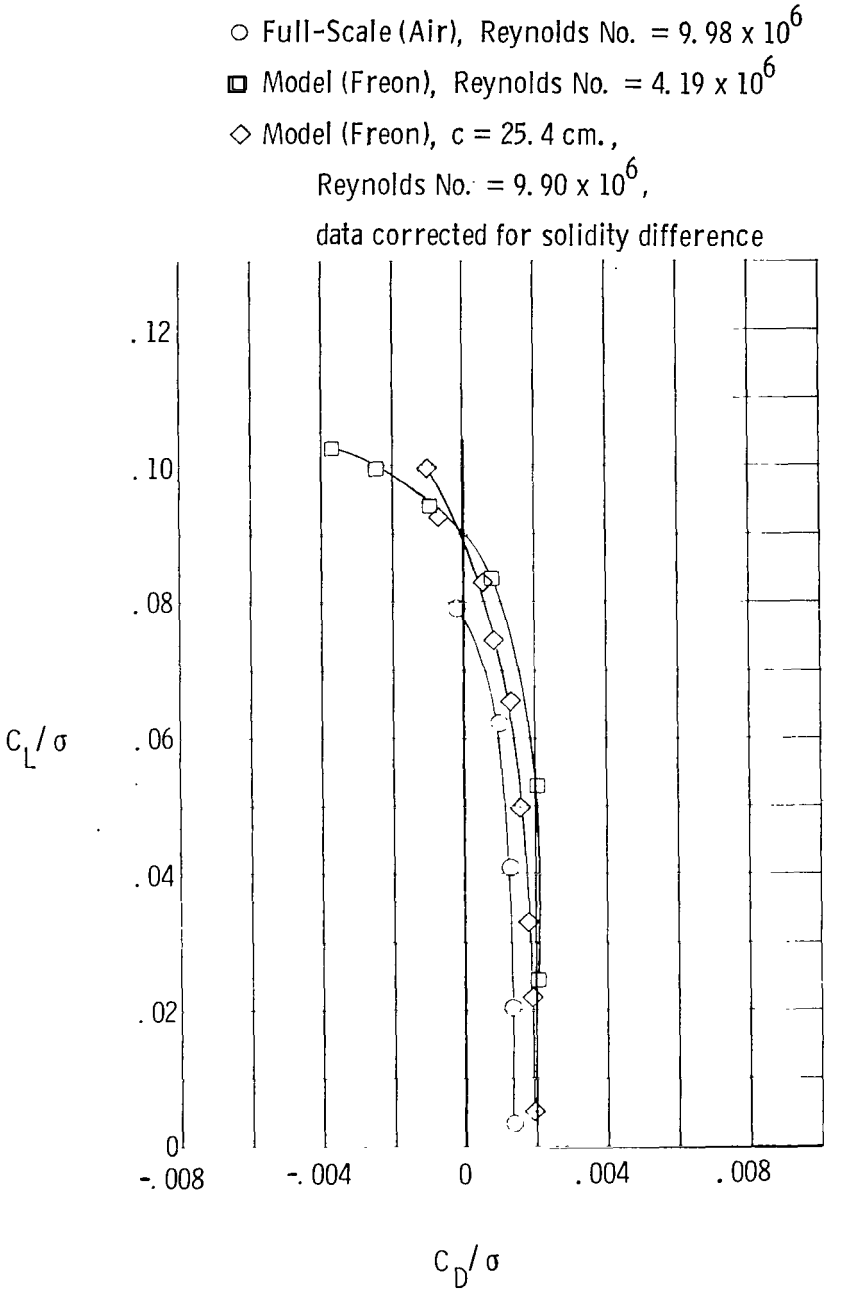

(a) $\mu = 0.30$, $M_{(1.0,\ 90)} = 0.79$, $\alpha_{TPP} = 0^{o}$.

Figure 12.- Effect of scaling parameters on freon model and full-scale values of C_L/σ and C_D/σ.

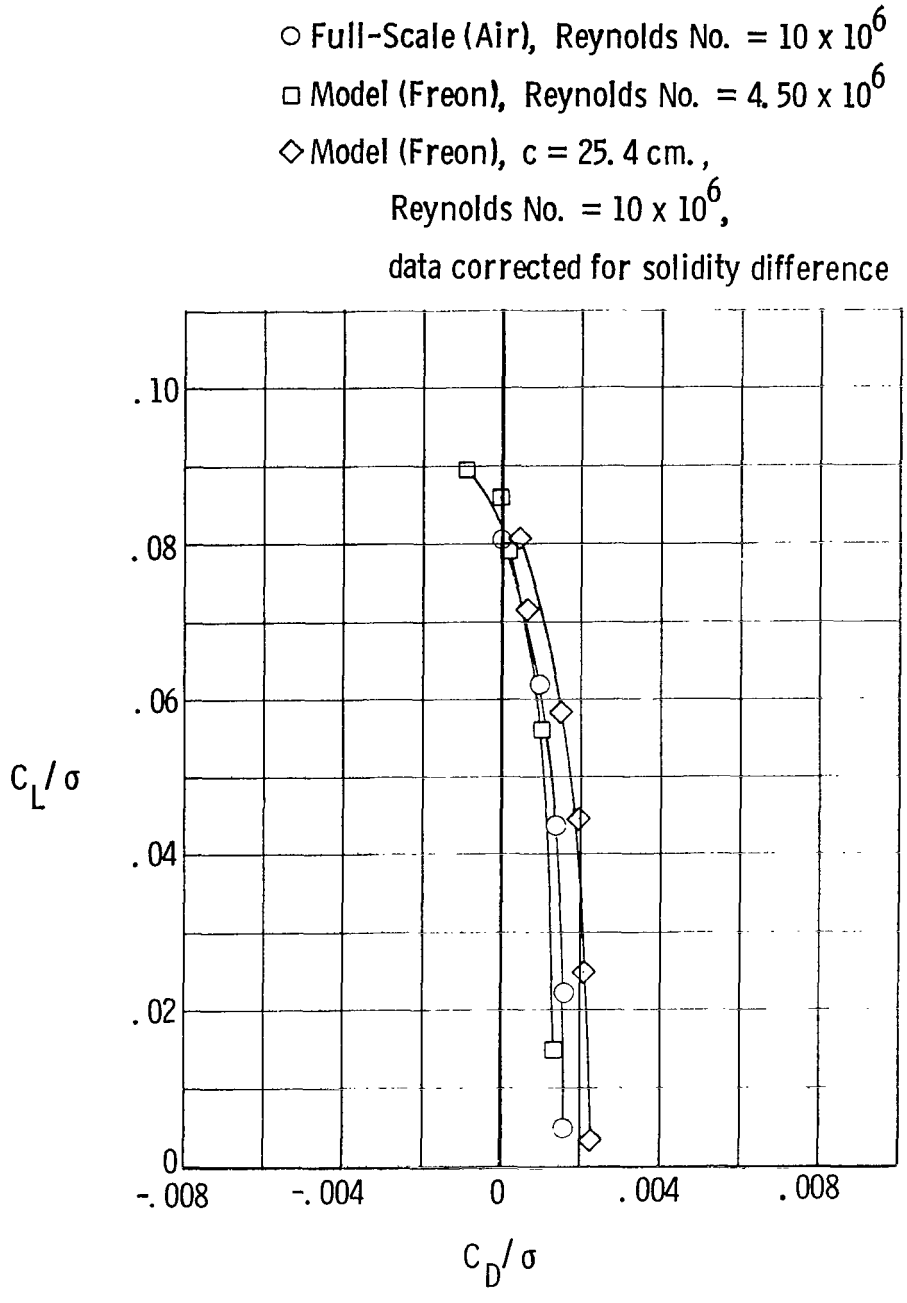

(b) $\mu = 0.30$, $M_{(1.0, 90)} = 0.85$, $\alpha_{TPP} = 0^{o}$.

Figure 12.- Continued.

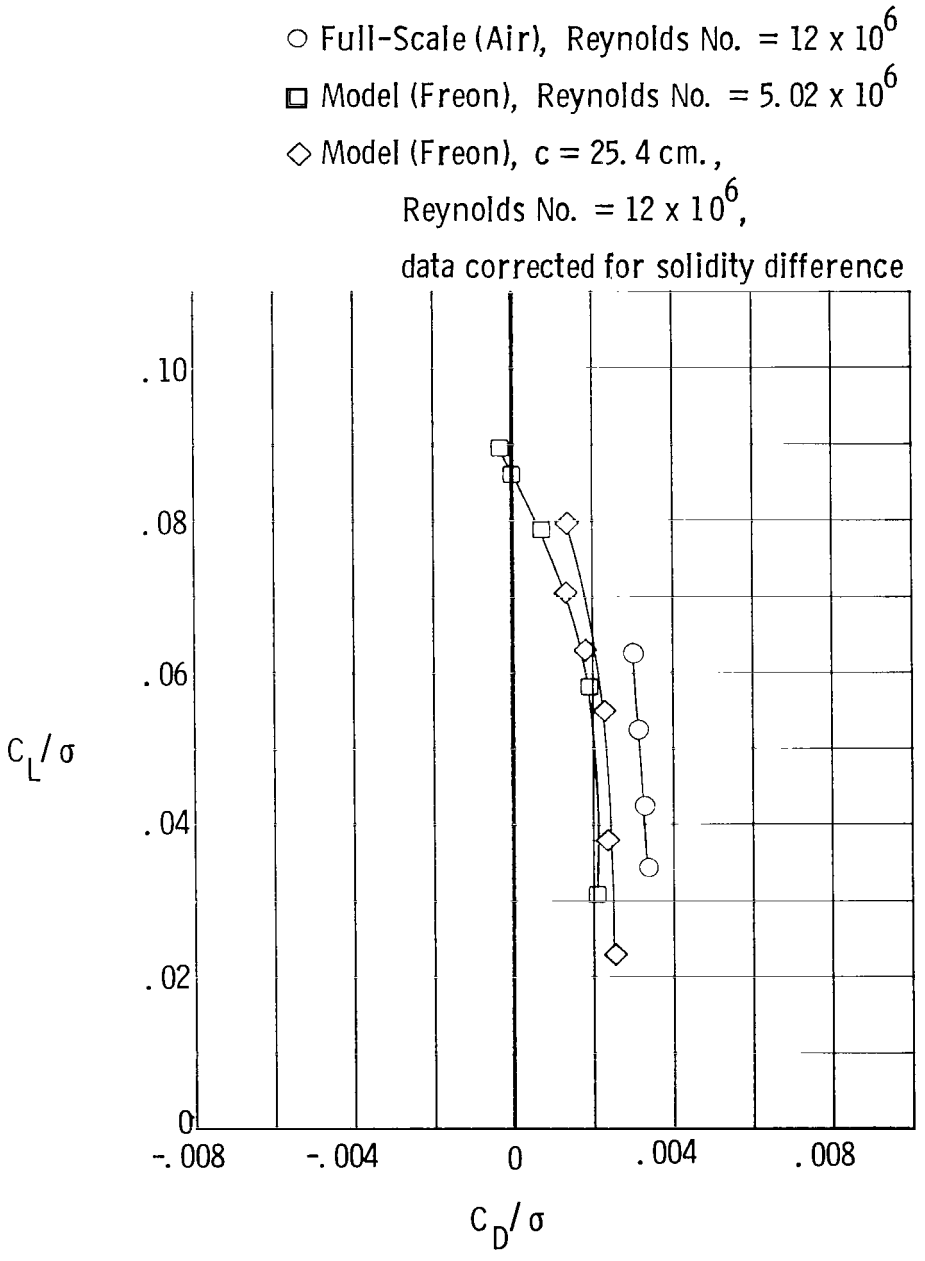

(c) $\mu = 0.30$, $M_{(1.0,\ 90)} = 0.95$, $\alpha_{TPP} = 0^{o}$.

Figure 12.- Continued.

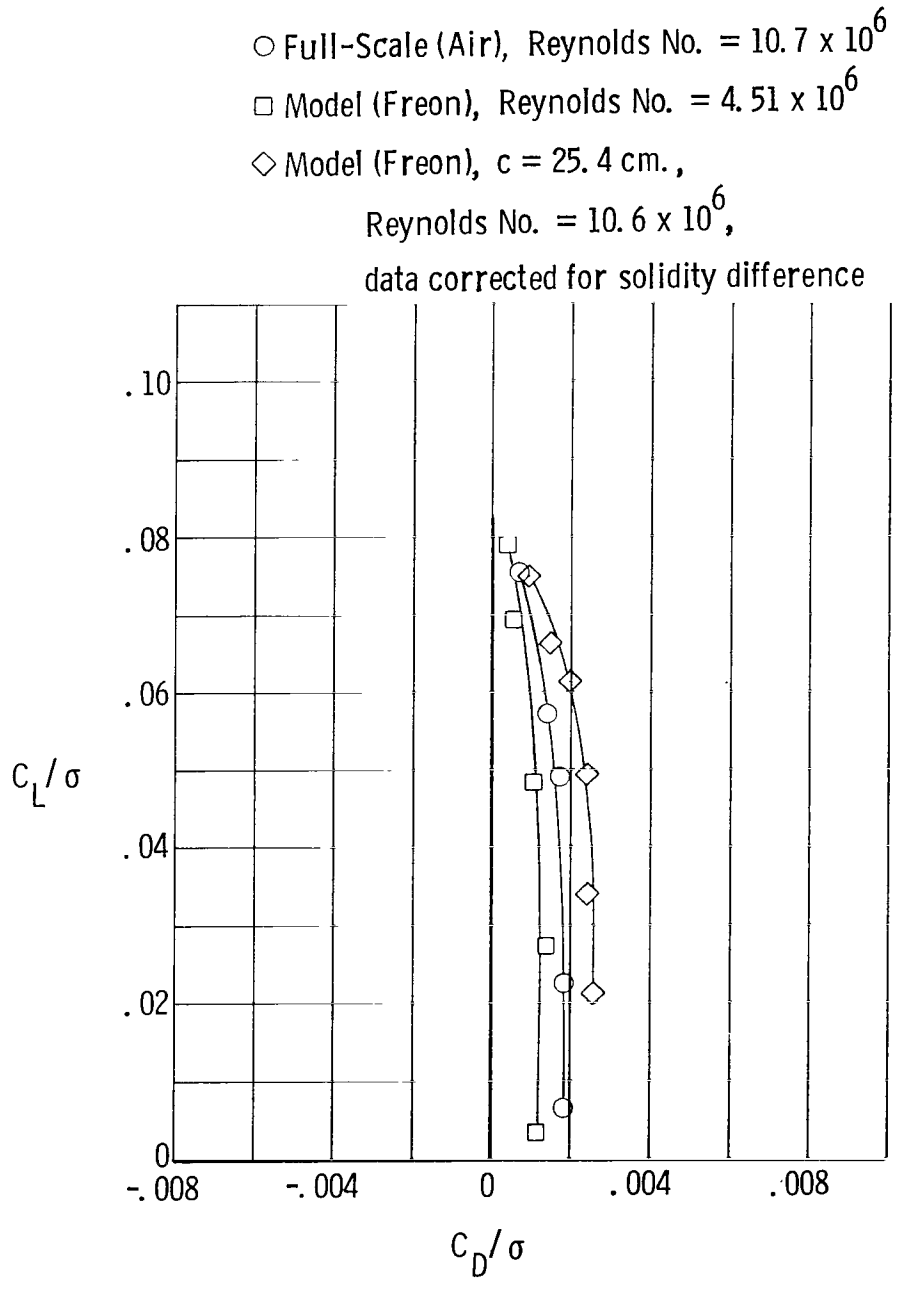

(d) $\mu = 0.35$, $M_{(1.0, 90)} = 0.85$, $\alpha_{TPP} = 0^{o}$.

Figure 12.- Continued.

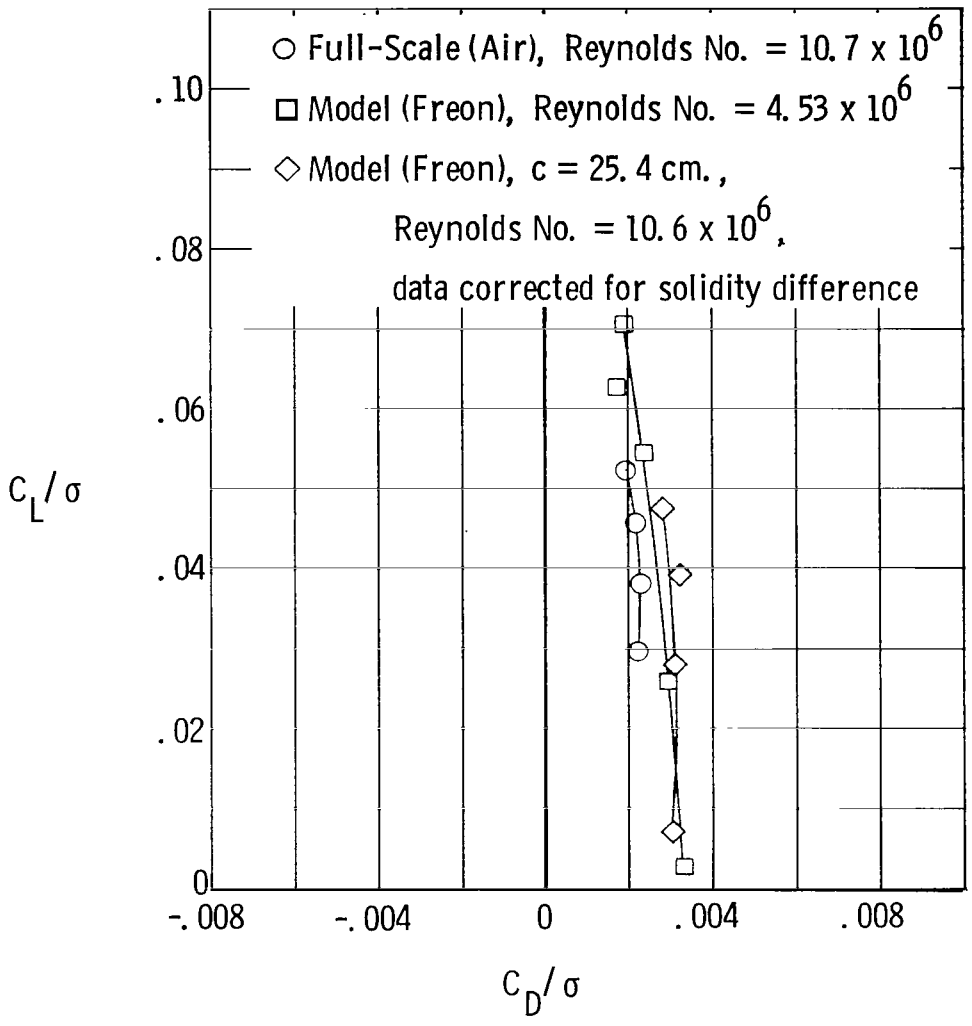

(e) $\mu = 0.40$, $M_{(1.0, 90)} = 0.85$, $\alpha_{TPP} = 0^{o}$.

Figure 12.- Concluded.

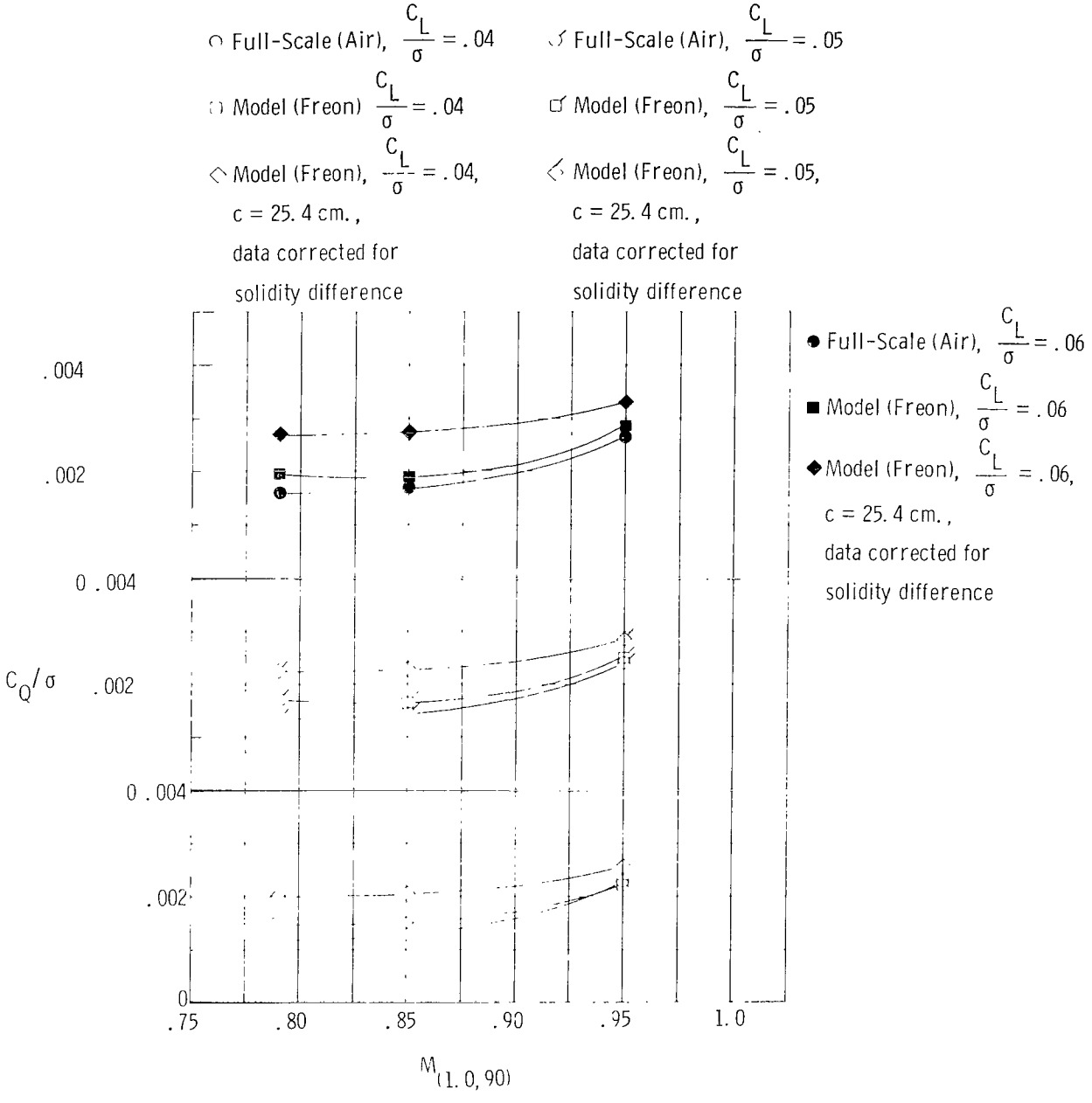

(a) $\mu = 0.30$, $\alpha_{TPP} = 0^{o}$.

Figure 13.- Effect of scaling parameters on freon model and full-scale performance for increasing $M_{(1.0, 90)}$ and μ.

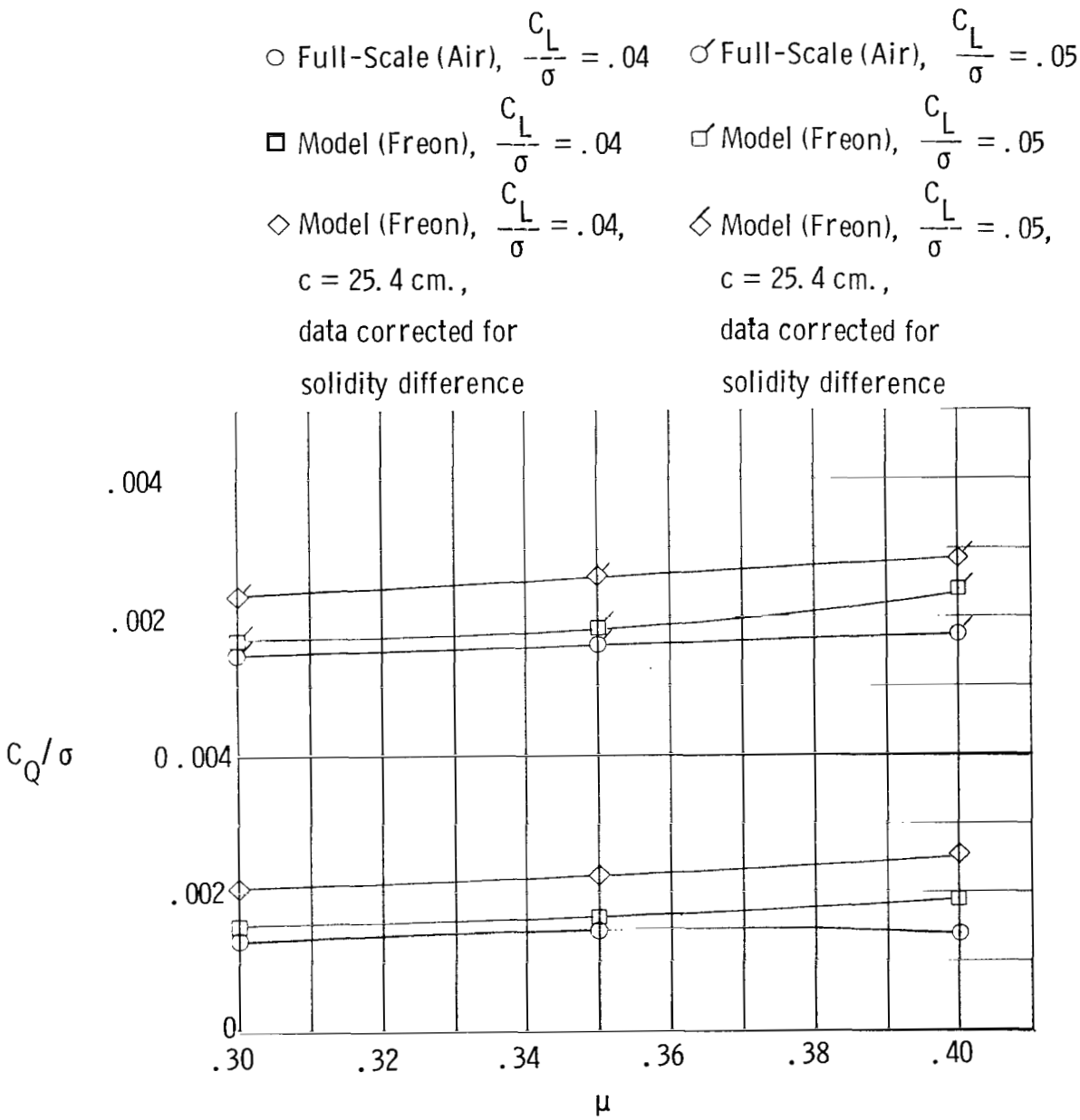

(b) $M_{(1.0, 90)} = 0.85$, $\alpha_{TPP} = 0^{o}$.

Figure 13.- Concluded.

"The aeronautical and space activities of the United States shall be conducted so as to contribute . . . to the expansion of human knowledge of phenomena in the atmosphere and space. The Administration shall provide for the widest practicable and appropriate dissemination of information concerning its activities and the results thereof."

—NATIONAL AERONAUTICS AND SPACE ACT OF 1958

NASA SCIENTIFIC AND TECHNICAL PUBLICATIONS

TECHNICAL REPORTS: Scientific and technical information considered important, complete, and a lasting contribution to existing knowledge.

TECHNICAL NOTES: Information less broad in scope but nevertheless of importance as a contribution to existing knowledge.

TECHNICAL MEMORANDUMS: Information receiving limited distribution because of preliminary data, security classification, or other reasons. Also includes conference proceedings with either limited or unlimited distribution.

CONTRACTOR REPORTS: Scientific and technical information generated under a NASA contract or grant and considered an important contribution to existing knowledge.

TECHNICAL TRANSLATIONS: Information published in a foreign language considered to merit NASA distribution in English.

SPECIAL PUBLICATIONS: Information derived from or of value to NASA activities. Publications include final reports of major projects, monographs, data compilations, handbooks, sourcebooks, and special bibliographies.

TECHNOLOGY UTILIZATION PUBLICATIONS: Information on technology used by NASA that may be of particular interest in commercial and other non-aerospace applications. Publications include Tech Briefs, Technology Utilization Reports and Technology Surveys.

Details on the availability of these publications may be obtained from:

SCIENTIFIC AND TECHNICAL INFORMATION OFFICE

NATIONAL AERONAUTICS AND SPACE ADMINISTRATION

Washington, D.C. 20546